



Research article

Integrating computational methods and *in vitro* experimental validation reveals the pharmacological mechanism of *Selaginella bryopteris* (L.) Baker targeting major proteins in breast cancer

Amir Mahgoub Awadelkareem^a, Mitesh Patel^{b,*}, Humera Banu^a, Mohd Adnan^{c,*}^a Department of Clinical Nutrition, College of Applied Medical Sciences, University of Ha'il, Ha'il, P.O. Box 2440, Saudi Arabia^b Research and Development Cell, Department of Biotechnology, Parul Institute of Applied Sciences, Parul University, Vadodara, 391760, Gujarat, India^c Department of Biology, College of Science, University of Ha'il, Ha'il, P.O. Box 2440, Saudi Arabia

ARTICLE INFO

Keywords:

Breast cancer
Selaginella bryopteris
Network pharmacology
Molecular dynamics
EGFR
Secondary metabolites

ABSTRACT

Breast cancer remains a significant global health challenge, necessitating the exploration of novel therapeutic options. The present study employs an integrated approach encompassing network pharmacology, molecular docking, molecular dynamics simulations, and *in-vitro* validation to investigate the potential of *Selaginella bryopteris* in breast cancer treatment. Initial network pharmacology analysis revealed different potential targets and pathways associated with breast cancer that could be modulated by *S. bryopteris* phytochemical constituents. Molecular docking and dynamics simulations further elucidated the stability and dynamics of protein-ligand complexes (lanaroflavone-EGFR and sequoiaflavone-CTNNB1). The *in-vitro* assays demonstrated the ability of *S. bryopteris* crude extract to inhibit cancer cell growth (IC₅₀ - 78.34 µg/mL) migration and invasion, supporting the computational predictions. The integrated approach employed in the present study offers a robust framework for the systematic exploration of *S. bryopteris* in drug discovery as a promising candidate for breast cancer treatment.

1. Introduction

Worldwide, breast cancer is a major cause of death from cancer, especially among women [1,2]. There were approximately 2.3 million new cases of breast cancer in 2020, as well as 6,85,000 deaths associated with the disease [3]. The diseases comprise different types of histological subtypes, each with different characteristics and implications [4]. It can be classified into different subtypes such as, invasive lobular carcinoma, invasive ductal carcinoma and HER2-positive breast cancer [5]. This complexity highlights the need for precise diagnostic and therapeutic approaches tailored to individual patients profiles [6]. Despite significant progress in conventional therapies, such as surgery, chemotherapy, radiation, and targeted therapies, the quest for more efficacious and less toxic treatment strategies remains paramount [4,7].

Natural plant metabolites have been attracting attention in recent years for their potential to treat breast cancer [8–10]. The long history of using botanical remedies for various diseases, including cancer, shows the historical knowledge that natural compounds

* Corresponding author.

** Corresponding author.

E-mail addresses: patelmeet15@gmail.com (M. Patel), drmohdadnan@gmail.com (M. Adnan).

have bioactive properties with therapeutic potential [11,12]. Natural products have the benefit of diversity, with a huge number of compounds that have evolved to interact with biological systems, often targeting complex signaling pathways and processes [13,14]. At the present time, researchers are trying to discover novel treatment options via searching the complex biochemical pathways of natural secondary metabolites and their potentiality to influence important processes in different types of cancer. Such, natural secondary metabolites consist of several compounds including alkaloids, flavonoids, terpenoids, saponins, phenolics etc. which have various biological activities [15–18].

Selaginella bryopteris (*S. bryopteris*) belonging to the Selaginellaceae family has a wide range of medicinal applications in prevention and cure of several diseases including urinary tract infections, beri-beri, spermatorrhoea, leucorrhoea, venereal disease, epilepsy, colitis, fever, constipation and cancer [19,20]. Additionally, it is also known as a tonic to support longevity and vitality [21]. There are different types of phytochemical constituents present in *S. bryopteris* such as, bi-flavonoids, alkaloids, steroids, caffeoyl derivatives, secolignans, neolignans etc. which are reported for its antimicrobial, antiviral, antiparasitic, antioxidant, anti-inflammatory, anti-cancer and immunostimulatory activities [22–27]. The presence of such diverse phytochemical composition and bioactive potential of *S. bryopteris* stimulated the exploration of mechanism via which these phytochemical constituents exert their effects, potentially offering innovative avenues for breast cancer therapy.

Moreover, computational methods can be integrated into the process with biological data has given rise to the network pharmacology approach which is widely used now a days for the understanding of complex diseases specifically cancer [28]. Network pharmacology is a combination of computational biology, system biology and pharmacology which can provides a clear picture of possible interactions occurs between biological components inside living organisms [29]. In the field of cancer research, this approach has raised as an important and powerful tool to determine the multifaceted nature of the disease from the identification of molecular mechanisms responsible for tumorigenesis to the interconnected pathways which can be targeted for the treatment [28–30].

Thus, the present study sought to better understand and identify bioactive phytochemical constituents from *S. bryopteris* that may be useful in treating breast cancer. Through a comprehensive approach, the bioactive compounds of *S. bryopteris* were systematically examined using network pharmacology, molecular docking, and simulations. Moreover, further anticancer and anti-metastasis activities of *S. bryopteris* were also performed via different *in vitro* methods.

2. Materials and methods

2.1. Identifying the potential targets of compounds and diseases

The PubChem database was used to get the SMILES code of the phytochemical constituents of *S. bryopteris* that were reported in literature. The obtained SMILES codes were entered into the SwissTargetPrediction database [www.swisstargetprediction.ch/, accessed on August 26, 2023] [31] to get the predicted targets for the phytochemicals. The search for genes related to breast cancer was carried out using the GeneCards database [<https://www.genecards.org/>, August 26, 2023] with the keyword “breast cancer”. Further DisGeNET [<http://www.disgenet.org/>, accessed on August 26, 2023] and OMIM databases [<https://www.omim.org/>, accessed on August 26, 2023] were also used to find disease-associated targets. The cutoff of “score_gda >0.1” was used for DisGeNET and relevance score >30 was used for GeneCards.

2.2. ADMET prediction

The phytochemical constituents of *S. bryopteris* were screened according to their ADMET properties. Utilizing ADMETlab 2.0 (<https://admetmesh.scbdd.com/>), predictions of ADMET properties and PAINS patterns (Pan-assay interference compounds) were made [32]. For Drug likeness properties prediction, Molsoft server (<https://molsoft.com/mprop/>) has been used [33]. Compounds with good ADMET properties were filtered out in addition to drug likeness score and PAINS patterns. Through the PAINS filter, we are able to eliminate compounds that can bind to more than one target simultaneously and have specific patterns. Clinical trials are less likely to fail if a compound has drug-like physicochemical and pharmacokinetic properties. ADMET evaluates compounds based on their physicochemical and pharmacokinetic properties.

2.3. Finding and acquiring potential targets

The FunRich tool version 3.1.3 was used to search for common targets between phytochemical constituents of *S. bryopteris* and breast cancer [34]. Further information about possible protein targets was obtained from the Swiss target prediction database [https://www.http://www.swisstargetprediction.ch/error_page.php?error=1/search], which was accessed on August 26, 2023. The construction of Venn diagrams was carried out to visualize the common targets using FunRich tool [35].

2.4. Findings of hub-genes and construction and analysis of protein–protein interaction network

The Cytohubba plugin of Cytoscape (Version 3.10.1) was used to find the Hub genes in the network and the top ten hub-genes were selected based on the Degree method. The protein–protein interactions (PPIs) of the possible targets were investigated using the STRING database (<https://string-db.org/>, accessed on August 26, 2023) [36]. The confidence level was set at 0.400 and the false discovery rate (FDR) was set at 5 % for the analysis based on the parameter settings. The PPI network of the possible targets was built and analyzed using Cytoscape software (Version 3.10.1) [37]. The network was imported into Cytoscape from the STRING database.

The network nodes were characterized by three topological measures: “degree”, “betweenness centrality” and “closeness centrality”. These measures were used to select a range of possible targets.

2.5. GO-KEGG pathway enrichment analysis

The biological functions and pathways related to the target proteins and disease were analyzed using the DAVID database (<https://david.ncifcrf.gov/>, accessed on August 27, 2023) [38]. The enrichment analysis was done with a False Discovery Rate (FDR) of less than 0.05 and the results were visualized using GO terms and pathways. A bubble graph was created using SRplot (<https://www.bioinformatics.com.cn/>) to show the top ten most relevant GO terms (BP, CC, and MF) using bioinformatics tools. A top twenty KEGG pathway map was created using ShinyGo 0.77 server (<http://bioinformatics.sdstate.edu/go/>).

2.6. Molecular docking analysis

The binding affinity of phytochemical constituents of *S. bryopteris* to breast cancer targets was evaluated using AutoDock v1.5.7 [39]. The 3D structures of ligands were obtained from the PubChem database and converted from .sdf to .pdb using Open Babel v2.4.1 [40]. The structures were then optimized by energy minimization using Avogadro with MMFF94 force field and Steepest Descent algorithm for 5000 steps. The minimization was stopped when the energy difference was less than 0.1 and the structures were saved as .pdb files. The 3D crystal structures of the receptors were downloaded from RCSB-PDB database with the following PDB ID, EGFR (PDB ID:4ZAU), TP53 (PDB ID:3DCY), MAPK3 (PDB ID:3FHR), STAT3 (PDB ID:6QHD), VEGFA (PDB ID:4KZN), TNF (PDB ID:2AZ5), ESR1 (PDB ID:1A52), CTNNB1 (PDB ID:4HM9), AKT1 (PDB ID:3OCB). The water molecules and het atoms were removed from the receptors, polar hydrogen and Kollman charge were added. The protein structures were then saved as .pdbqt format. The protein-ligand complexes were docked using AutoDock Vina and visualized using PyMol and Biovia Discovery Studio [41].

2.7. Molecular dynamics simulation

To study the time-dependent conformational stability of ligands in the receptor binding pocket, computational methods such as molecular dynamics (MD) was employed. MD has been shown to be useful for finding new inhibitors in various applications [42–45]. The MD simulations were done using Gromacs version 2019.4 [46] with the CHARMM force field. The ligand topology was obtained from the SwissParam server and used to generate the force field parameters. The system was vacuum minimized for 1500 steps using the steepest descent algorithm. The protein–ligand complex was then immersed in a cubic periodic box of 0.5 nm with TIP3P water model. The system was neutralized by adding Na^+ and Cl^- counterions to achieve a salt concentration of 0.15 M. The NVT equilibration steps were performed for 100 ps each using the leap-frog algorithm. The production MD run was carried out for 100 ns on the solvated protein–ligand complex. The trajectory file was processed to remove the periodic boundary conditions from the MD simulation. The MD data was analyzed using the Chimera package and the graphs were created using the XMGRACE tool (<https://plasma-gate.weizmann.ac.il/Grace/>) [47,48].

2.8. Principal component analysis and free energy landscapes

A convenient way to explore protein conformational sampling is through principal component analysis (PCA) [49]. In order to determine their principal motions via PCA, the MD trajectories of EGFR-lanarflavone and CTNNB1-sequoiaflavone were examined. PCA was performed using the essential dynamics (ED) method by diagonalizing the first two eigenvectors (EVs) of covariance matrix [50]. Moreover, to examine their stability and folding dynamics, free energy landscapes (FELs) for EGFR-lanarflavone and CTNNB1-sequoiaflavone complex were generated. A conformational sampling approach was employed to generate FELs, which helps understand the conformational stability EGFR-lanarflavone and CTNNB1-sequoiaflavone complex during the simulation.

2.9. MM-PBSA calculations

The binding of lanaraflavone with EGFR and sequoiaflavone with CTNNB1 was further checked by utilizing the MMPBSA approach to calculate the docked complex's binding affinity [51]. The MM–PBSA analysis was conducted using the *g_mmpbsa* package of GROMACS [52].

2.10. Collection of plant material and extract preparation

The plants of *S. bryopteris* was collected from the local market. A voucher specimen (BVBR512) was deposited at Bapalal Vaidya Botanical Research Centre, Department of Biosciences, Veer Narmad South Gujarat University, Surat, Gujarat, India. The whole plant was dried, ground into a fine powder using an electric grinder and stored in an airtight container. Prior to the preparation of the crude extract, the percentage yield of the extract was determined using various solvents. For this, plant powder (1 g) was soaked in 10 mL of different solvents (chloroform, ethyl acetate, n-butanol, 85 % ethanol and water) based on their increasing polarity and kept under vigorous shaking at 110 rpm at 37 °C. On the next day, the solvent phase was filtered with the Whatman No. 1 filter paper for obtaining crude extract and the yield of the extract was calculated. Afterwards, plant powder powder (10 g) was further soaked in 200 mL of 85 % ethanol and shaken at room temperature for 24 h. The ethanol extract was filtered through Whatman No. 1 filter paper and

concentrated by rotary evaporation at 45 °C. The crude extract was further dried in a water bath at 45 °C until a constant weight was obtained.

2.11. Cell culture

Breast cancer cells (MCF-7) were cultured in a medium containing DMEM, FBS (10 %), streptomycin (5 mg) and penicillin (10,000 units). Humidity and 5 % CO₂ conditions were maintained at 37 °C for the cells to ensure their optimal growth [53]. The breast cancer cell line was derived from the National Centre for Cell Science (NCCS), Pune, India.

2.12. Cell viability assay

Breast cancer cells were tested by MTT assay for viability when exposed to crude extract of *S. bryopteris*. Trypsinization and aspiration were used to remove cells from T-25 flasks and then cells were collected via centrifugation at 3000 rpm. A density of 10,000 cells per 200 µL was adjusted in culture medium after resuspending the cells. To allow the cells to adhere, 200 µL of cell suspension was added to each well of a 96-well plate and incubated for 24 h at 37 °C with 5 % CO₂ conditions. Then, the medium was discarded and the cells were treated with 200 µL of various concentrations of *S. bryopteris* crude extract (1, 10, 100, 250, 500 and 1000 µg/mL) for another 24 h at the same conditions. After that, 200 µL of fresh medium containing 10 % MTT reagent was added to each well and incubated for 3 h at 37 °C with 5 % CO₂. The formazan crystals that formed were dissolved by adding 100 µL of DMSO and shaking gently. The absorbance was measured at 570 nm and 630 nm using a microplate reader. The IC₅₀ value, which is the concentration of *S. bryopteris* crude extract that inhibits 50 % of the cell growth was determined by subtracting the background and blank values [54, 55]. The standard drug paclitaxel was used as a positive control and DMSO was used as a negative control.

2.13. Wound healing assay

To determine the effect of crude extract of *S. bryopteris* on the migration of MCF-7 cancer cells, wound-healing assays was conducted. Cells were seeded at a concentration of 1×10^6 cells/mL in 3 mL of medium in 6-well plates and allowed to form a monolayer. Using a sterile 1 mL pipette tip, scratch was made in each well. An inverted microscope was used to measure the initial width of scratch. Then, *S. bryopteris* crude extract was added to the wells at IC₅₀ concentration and the plates were incubated for 44 h. The final scratch width was again measured and compared to the initial scratch width. In the case of a decrease in the width of the scratch, this indicates that the cells are capable of migrating and healing the scratch [56].

2.14. Transwell migration assay

The effect of *S. bryopteris* crude extract on the invasion of MCF-7 cancer cells was evaluated using Transwell inserts (24-well format, 8 µm pore size, Himedia®, India). The cells were suspended in serum-free media and seeded at a density of 1×10^6 cells in the upper chamber of the inserts. The lower chamber was filled with media containing 10 % FBS as a chemoattractant. The cells were treated with IC₅₀ concentrations of *S. bryopteris* crude extract and incubated for 10 h. The cells that did not invade through the membrane were removed with a cotton swab. The cells that invaded to the lower surface of the membrane were fixed with methanol and stained with crystal violet (0.1 %). The number of invaded cells was counted under an inverted microscope by averaging three random fields per well [57].

3. Results

3.1. Screening of phytochemical compounds of *S. bryopteris* and ADMET analysis

This study extracted 13 phytochemical constituents from the existing literature that were identified in *S. bryopteris*. Through ADMETlab 2.0 and Molsoft web server, the ADMET properties, PAINS patterns and drug-likeness properties of all selected compounds were predicted. Tables 1 and 2 provide the ADMET properties of all the compounds. According to the results, ten compounds exhibit good drug-like properties without showing any PAINS patterns. The analysis of 13 compounds was limited to three compounds with drug-likeness properties less than 0.18, disqualifying them from further assessment. ADMET properties revealed that ten compounds (Amentoflavone, 2,3-Dihydro amentoflavone, Tetrahydro-amentoflavone, 2,3-Dihydro hinokiflavone, Tetrahydro-hinokiflavone, Lanaroflavone, Sequoiaflavone, β-sitosterol, Heveaflavone, β-sitosterol β-D-glucoside) shared a similar class of ADMET properties without any toxic patterns. According to ADMET properties, these ten compounds have the potential to be a potent and safe anticancer drug lead.

3.2. Prediction of targets and screening of potential targets

Detailed information was accessed from the PubChem database, while the SwissTargetPrediction (STP) database was employed to analyse the target classes associated with each of these compounds. The target classes of each phytochemical constituents of *S. bryopteris* passing ADMET criteria is presented in Figure-1(A-J). Total 406 predicted targets for the phytochemical constituents of *S. bryopteris* were obtained from the Swisstarget prediction whereas, 2060 predicted targets from Genecards (GDA cutoff of >30),

Table 1List of phytochemical constituents of *S. bryopteris* and their ADMET analysis (chemical absorption, distribution, metabolism, excretion and toxicity).

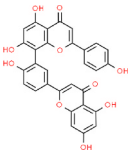
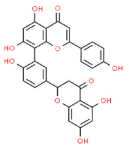
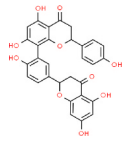
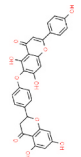
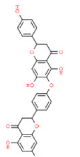
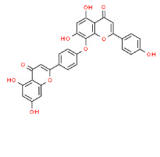
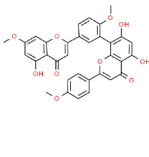
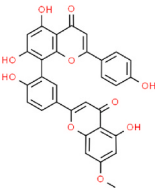
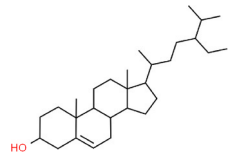
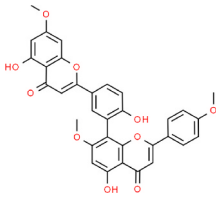
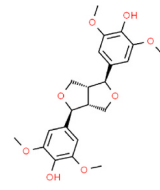
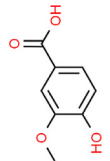
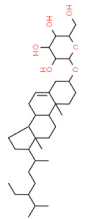
Details	Amentoflavone	2,3-Dihydro amentoflavone	Tetrahydro-amentoflavone	2,3-Dihydro hinokiflavone	Tetrahydro-hinokiflavone	Lanaroflavone	Sciadopitysin
Structure							
Pubchem ID	5281600	16066857	326004	71437113	101938918	11272651	5281696
MF	C30H18O10	C30H20O10	C30H22O10	C30H20O10	C30H22O10	C30H18O10	C33H24O10
MW	538.5 g/mol	540.5 g/mol	542.5 g/mol	540.5 g/mol	542.5 g/mol	538.5 g/mol	580.5 g/mol
Druglikeness	0.19	0.69	0.67	1.13	0.98	0.68	0.13
LogP	6.003	5.575	4.999	5.276	4.711	5.757	6.683
Pgp-inh	0.02	0.026	0.012	0.035	0.074	0.034	0.978
Pgp-sub	0.016	0.001	0.004	0.004	0	0.018	0.112
F(20 %) Bioavailability	0.999	0.99	0.998	0.94	0.42	0.977	0.022
F(30 %) Bioavailability	1	1	1	1	0.997	1	1
Caco-2	-5.263	-5.418	-5.76	-5.053	-5.677	-5.13	-4.993
BBB	0.001	0.001	0.002	0.002	0.005	0.001	0
PPB	96.92 %	98.14 %	98.05 %	99.49 %	99.63 %	98.47 %	91.27 %
CYP2D6-inh	0.109	0.084	0.155	0.14	0.133	0.117	0.045
CL	3.819	6.645	5.79	5.123	12.056	4.04	3.842
hERG	0.096	0.052	0.131	0.083	0.067	0.066	0.051
DILI	0.988	0.987	0.965	0.973	0.97	0.982	0.985
Ames	0.258	0.653	0.466	0.601	0.527	0.39	0.303
ROA	0.068	0.769	0.519	0.942	0.971	0.56	0.054
IGC50	5.194	5.485	5.242	5.418	5.649	5.113	5.463
LC50	5.468	6.204	6.149	6.625	7.167	5.984	6.323
nHA	10	10	10	10	10	10	10
nHD	6	6	7	5	5	5	3
TPSA	181.8	177.89	181.05	166.89	162.98	170.8	148.8
nRot	3	3	3	4	4	4	6
nRing	6	6	6	6	6	6	6
SureChEMBL	0	0	0	0	0	0	0
QED	0.177	0.181	0.165	0.197	0.225	0.192	0.213
PAINS	0	0	0	0	0	0	0
Lipinski violation	2	2	2	1	1	1	1

Table 2

List of phytochemical constituents of *S. bryopteris* and their ADMET analysis (chemical absorption, distribution, metabolism, excretion and toxicity).

Details	Sequoiainone	β -sitosterol	Heveaflavone	(+)-Syringaresinol	Vanillic Acid	β -sitosterol β -D-glucoside
Structure						
Pubchem ID	5484010	222284	15559724	443023	8468	12309060
MF	C31H20O10	C29H50O	C33H24O10	C22H26O8	C8H8O4	C35H60O6
MW	552.5 g/mol	414.7 g/mol	580.5 g/mol	418.4 g/mol	168.15 g/mol	576.8 g/mol
Druglikeness	0.27	0.78	0.59	-0.61	-0.18	0.5
LogP	6.357	7.663	6.565	1.993	1.396	5.97
Pgp-inh	0.088	0.341	0.976	0.238	0.001	0.248
Pgp-sub	0.042	0.001	0.095	0.147	0.003	0.004
F(20 %) Bioavailability	0.925	0.01	0.024	0.008	0.01	0.015
F(30 %) Bioavailability	1	0.233	1	0.055	0.655	0.158
Caco-2	-5.175	-4.756	-4.96	-4.784	-5.159	-4.785
BBB	0.001	0.84	0	0.038	0.439	0.059
PPB	96.60 %	98.31 %	90.18 %	82.05 %	53.17 %	97.24 %
CYP2D6-inh	0.092	0.005	0.031	0.091	0.015	0
CL	3.707	16.686	3.927	6.418	7.899	5.939
hERG	0.072	0.049	0.045	0.178	0.031	0.04
DILI	0.987	0.203	0.985	0.227	0.857	0.085
Ames	0.321	0.026	0.321	0.084	0.015	0.068
ROA	0.067	0.018	0.059	0.16	0.053	0.039
IGC50	5.344	4.984	5.48	4.771	2.662	4.917
LC50	5.817	5.365	6.476	5.708	2.88	5.307
nHA	10	1	10	8	4	6
nHD	5	1	3	2	2	4
TPSA	170.8	20.23	148.8	95.84	66.76	99.38
nRot	4	6	6	6	2	9
nRing	6	4	6	4	1	5
SureChEMBL	0	0	0	0	0	0
QED	0.19	0.436	0.213	0.738	0.693	0.257
PAINS	0	0	0	0	0	0
Lipinski violation	1	1	1	0	0	1

DisGeNet (cutoff of >0.1) and OMIM databases were obtained for breast cancer after removing duplicates. A total of 163 common targets were retrieved as potential targets among the obtained targets of compounds and diseases (Figure-2).

3.3. Finding of hub genes and construction of compounds-disease common target network

Data on potential target genes and their interactions were obtained from the STRING database. Then, Cytoscape version 3.10.1 was used to visualize and analyse the data as a PPI network. Common gene network and compound target network has been created (Figure-3 and 4). A cytoNCA plugin was used to determine the significance of each node in the network, with three parameters such as degree, closeness and centrality of the nodes (Table-3 and 4). Based on these parameters, we can determine how important each node is to the rest of the network. It was found that the target genes obtained were involved in the progression of breast cancer. There is a possibility that these key targets may play a role in the anti-cancer activity of phytochemical constituents of *S. bryopteris*. The top ten hub genes have been identified by using cytohubba plugin in Cytoscape by using degree-finding method. Based on the ranking of the ten most significant targets in the network, we found that the top ten targets that had the highest values of the parameters were EGFR, TP53, TNF, TNF, STAT3, VEGFA, ESRI, CTNNB1, AKT1 and SRC (Figure-5A). Breast cancer may be prevented by modulating these ten targets by *S. bryopteris* phytochemical constituents. A further level of analysis was conducted with GeneMANIA to determine how the target genes relate to other genes in the network. Interactions in the network are weighted differently based on their type, according to the results. Among the most common types of interactions, there were genetic interactions (7.02 %), predicted interactions (5.51 %), colocalization interactions (5.51 %), co-expression interactions (14.98 %) and physical interactions (65.23 %) (Figure-5B).

3.4. Functional and pathway enrichment analysis

DAVID database was used to understand the functions, pathways and the involvement of identified targets in the breast cancer. A better understanding of the general mechanism behind the disease would be gained as a result. Target genes were found to associated with numerous GO enrichment terms based on the GO annotations. A total of 814 BPs, 82 CCs, and 135 MFs were identified. For each GO category, a bubble chart was used to display the top ten enriched terms (Fig. 6A–C) and each KEGG pathways (Fig. 6D). Genes associated with biological processes were discovered to be involved in protein autophosphorylation, cellular response to chemical stress, regulation of epithelial cell proliferation, activation of protein kinase activity, muscle cell proliferation, peptidyl-serine phosphorylation, cellular response to oxidative stress, peptidyl-tyrosine phosphorylation, in different cellular component such as membrane raft, membrane microdomain, adherens junction, postsynaptic density, asymmetric synapse, caveola with different molecular functions such as, protein phosphatase binding, nuclear receptor binding, estrogen receptor binding, hormone receptor binding, ATPase binding, etc. These genes were found to associated with 143 KEGG pathways. Pathways that were significantly enriched in this study included resistance to EGFR tyrosine kinase inhibitors, prolactin signaling pathways, HIF-1 signaling pathways, Rap1 signaling pathways and pathways related to cancer and breast cancer. These results suggest that phytochemicals of *S. bryopteris* can modulate may be able to modulate some signaling pathways in breast cancer.

3.5. Molecular docking analysis

S. Bryopteris phytochemical constituents were docked against breast cancer targets in Figure-7. Phytochemical binding energies and target protein binding energies indicate the stability of their interactions. Low binding energies lead to more stable interactions. The docking analysis revealed that some phytochemicals had significant affinity for their respective target proteins. The results of sequoiaflavone showed good binding energy towards CTNNB1 (-10.0 kcal/mol) showing two conventional hydrogen bond (TYR536 and GLN494), two carbon hydrogen bond (PRO364 and ALA412), one pi-sigma bond (TYR498), one pi-pi stacked bond (PHE491), one alkyl bond (ARG416) and two pi-alkyl bond (2*ILE362), towards AKT1 (-9.9 kcal/mol) with two conventional hydrogen bond

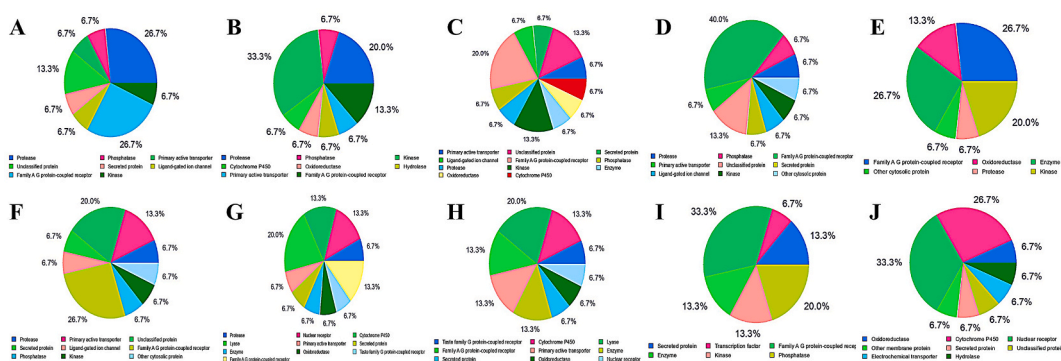


Fig. 1. The protein classification of targets of phytochemical constituents of *S. bryopteris* against breast cancer as retrieved from the SwissTargetPrediction server. (A). 2,3-dihydroamentoflavone, (B). 2,3-dihydrohinokiflavone, (C). Amentoflavone, (D). Heveaflavone, (E). Lanaroflavone (F). Sequoiaflavone, (G). Tetrahydro-amentoflavone, (H). Tetrahydro-hinokiflavone, (I). β -sitosterol β -D-glucoside, (J). β -sitosterol.



Fig. 2. Findings of common targets between phytochemical constituents of *S. bryopteris* and breast cancer by creating Venn diagram using Fun- Rich tool.

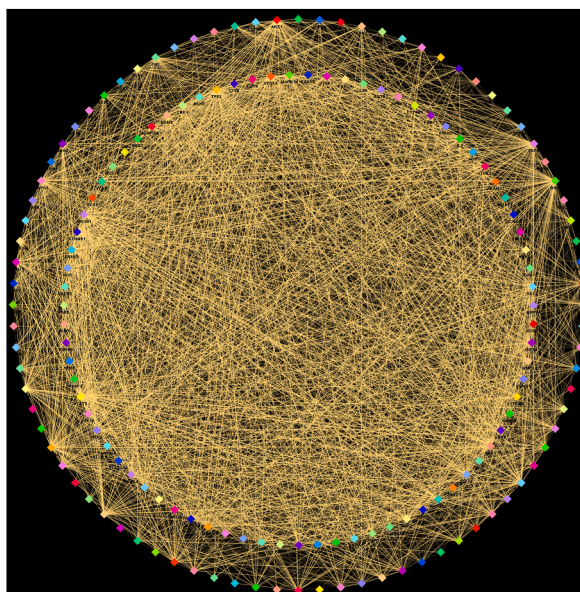


Fig. 3. The network of common-gene targets for breast cancer and phytochemical constituents of *S. bryopteris* created with Cytoscape software.

(LYS158 and LEU156), one carbon hydrogen bond (GLY294), two pi-anion bond (GLU234 and MET281), two pi-sigma bond (ASP292 and VAL164), four pi-alkyl bond (MET227, 2*VAL164 and LEU295) and one pi-sulfur bond (ALA177), towards TP53 (−9.9 kcal/mol) with two conventional hydrogen bond (GLN23 and ILE21), one carbon hydrogen bond (SER228), one pi-donor hydrogen bond (ARG203), one alkyl bond (LYS20) and ten alkyl bond (3*PRO115, 2*LEU100, ILE22, LYS20, LEU125, ALA200 and ARG203), Amentoflavone showed good binding energy towards SRC (−9.9 kcal/mol) showing two conventional hydrogen bond (THR338 and ILE336), one pi-sigma bond (VAL281) and six pi-alkyl bond (3*VAL281, 2*LYS295 and ALA293), towards STAT3 (−9.8 kcal/mol) showing two conventional hydrogen bond (LYS383 and GLU415), one carbon hydrogen bond (GLY421) and three pi-alkyl bond (2*LYS383 and LEU378), towards ESR1 (−9.8 kcal/mol) showing three conventional hydrogen bond (GLU323, ILE326 and LEU320), two carbon hydrogen bond (GLY390 and LYS449), one pi-anion bond (GIU353), one pi-donor hydrogen bond (ILE326), one pi-sigma bond (TRP393), one pi-pi t shaped bond (TRP393) and four pi-alkyl bond (ARG394, 2*PRO324 and ILE326), 2,3-Dihydroamentoflavone showed good binding energy towards TNF (−8.6 kcal/mol) showing one conventional hydrogen bond (ALA111), one carbon hydrogen bond (TRP114), two pi-sulfur bond (2*CYS69), one pi-pi stacked bond (TRP114) and two pi-alkyl bond (LYS112 and ALA111), towards VEGFA (−8.2 kcal/mol) with two conventional hydrogen bond (TYR25 and CYS104), one pi-anion bond (GLU103) and pi-pi stacked bond (2*TYR25), Lanaroflavone showed good binding energy towards EGFR (−10.4 kcal/mol) showing two conventional hydrogen bond (ASN842 and LEU718), one pi-donor hydrogen bond (THR790), one pi-sigma bond (VAL726), two pi-pi stacked bond (2*PHE723), one pi-pi t shaped bond (PHE723) and eight pi-alkyl bond (2*ALA743, 3*VAL726, LEU844, LEU718 and LYS745) and 2,3-Dihydrohinokiflavone showed good binding energy towards MAPK3 (−9.5 kcal/mol) showing three

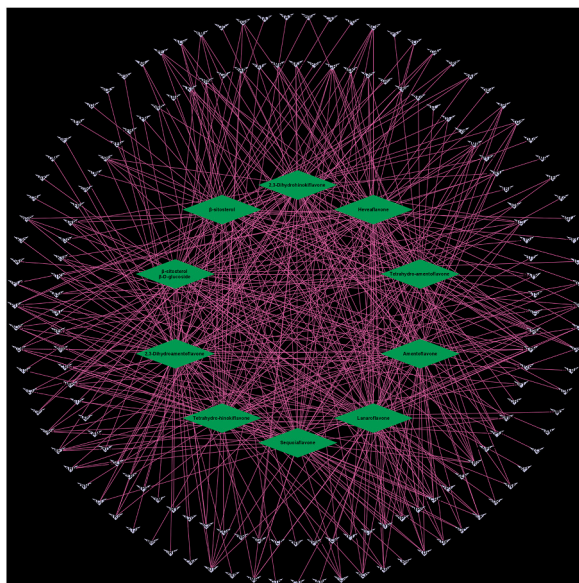


Fig. 4. The common-gene targets for phytochemical constituents of *S. bryopteris* (green diamonds) and their associations (pink edges) with the genes involved in breast cancer (light violet 'V' shape), visualized using cytoscape software. (For interpretation of the references to color in this figure legend, the reader is referred to the Web version of this article.)

Table 3

Topological parameters of phytochemical constituents of *S. bryopteris*.

Sr. No.	Compounds	Degree	Betweenness	Closeness
1	2,3-Dihydrohinokiflavone	49	3914.4412	0.4205379
2	β -sitosterol β -D-glucoside	48	9284.905	0.41849148
3	Sequoiافلانون	46	2603.8828	0.41445783
4	Lanaroflavone	46	2414.6377	0.41445783
5	2,3-Dihydroamentoflavone	46	6851.0146	0.41445783
6	Tetrahydro-hinokiflavone	42	4585.343	0.4066194
7	Heveافلانون	42	1975.486	0.4066194
8	Tetrahydro-amentoflavone	38	4646.576	0.39907193
9	Amentoflavone	38	1729.504	0.39907193
10	β -sitosterol	37	6312.2095	0.39722863

conventional hydrogen bond (LYS179, LYS177 and TYR174), one pi-anion bond (ASP149) and two pi-alkyl bond (ILE146 and ARG129). The interaction analysis of phytochemical constituents of *S. bryopteris* with target proteins are presented in Figs. 8 (A – D), 9 (A – D), 10 (A – D), 11(A – D) and 12 (A – D), as well as in Table 5.

3.6. MD simulation analysis

To elucidate the stability of the interactions between ligands and proteins, docked complexes of lanaroflavone with EGFR and sequoiaflavone with CTNNB1, which exhibited the highest binding energies in the molecular docking analysis were run for MD analysis. MD simulations were conducted over 100 ns using the GROMACS software. The structural deviations of the proteins and ligand-protein complexes were analyzed using Root Mean Square Deviation (RMSD) analysis to assess their stability and movement in the solvent environment. Throughout the simulations, both the EGFR-lanaroflavone and CTNNB1-sequoiaflavone complexes displayed stable RMSD patterns, indicating consistent backbone structures (see Figure-13A and Figure-14A). The average RMSD values for the EGFR backbone and the EGFR-lanaroflavone complex were 0.41 nm and 0.48 nm, respectively. Similarly, the average RMSD values for the CTNNB1 backbone and the CTNNB1-sequoiaflavone complex were 0.33 nm and 0.36 nm, respectively. These results suggest that both complexes-maintained stability throughout the simulation period, indicating strong ligand-protein interactions. The Root Mean Square Fluctuation (RMSF) serves as a measure of flexibility for individual residues within a protein. In the EGFR-lanaroflavone complex (Figure-13B), there was an average fluctuation of 0.14 nm, while in the CTNNB1-sequoiaflavone complex (Figure-14B), the average fluctuation was 0.17 nm during the simulation. Notably, upon binding with lanaroflavone and sequoiaflavone, these fluctuations appeared to stabilize and minimize. The graphical representation suggests that EGFR and CTNNB1, when bound with lanaroflavone and sequoiaflavone respectively, maintain consistent interactions with remarkable stability. The stability and integrity of protein structures rely significantly on hydrogen bonds (H-bonds). To evaluate these aspects in protein-ligand complexes, it's

Table 4
Topological parameters of Common Genes related to *S. bryopteris* and breast cancer.

Sr. No.	Genes	Description	Degree	Betweenness	Closeness
1	AKT1	AKT serine/threonine kinase 1	119	1888.3074	0.78640777
2	TP53	tumor protein p53	112	1187.5243	0.7570093
3	VEGFA	Vascular endothelial growth factor A	107	950.9138	0.739726
4	EGFR	epidermal growth factor receptor	105	965.6551	0.7330317
5	TNF	tumor necrosis factor	104	1475.5771	0.7330317
6	CTNNB1	catenin beta 1	101	975.15045	0.72
7	ESR1	estrogen receptor 1	98	1429.9392	0.7105263
8	STAT3	signal transducer and activator of transcription 3	94	570.78436	0.69827586
9	SRC	SRC proto-oncogene, non-receptor tyrosine kinase	94	679.9602	0.69827586
10	MAPK3	mitogen-activated protein kinase 3	94	645.6745	0.69827586
11	JUN	Jun proto-oncogene, AP-1 transcription factor subunit	89	405.7873	0.6835443
12	HSP90AA1	heat shock protein 90 alpha family class A member 1	87	702.9155	0.67782426
13	HIF1A	hypoxia inducible factor 1 subunit alpha	86	551.0334	0.675
14	ERBB2	erb-b2 receptor tyrosine kinase 2	83	698.978	0.6694215
15	PTGS2	prostaglandin-endoperoxide synthase 2	76	695.0671	0.648
16	MMP9	matrix metalloproteinase 9	71	272.17374	0.63529414
17	PPARG	peroxisome proliferator activated receptor gamma	71	979.0117	0.63779527
18	PIK3CA	phosphatidylinositol-4,5-bisphosphate 3-kinase catalytic subunit alpha	65	132.3177	0.6136364
19	BCL2L1	BCL2 like 1	65	300.43286	0.6230769
20	FGF2	fibroblast growth factor 2	62	147.03635	0.61132073
21	MDM2	MDM2 proto-oncogene	61	150.8388	0.60902256
22	EP300	E1A binding protein p300	61	169.0465	0.61132073
23	SIRT1	sirtuin 1	61	258.09766	0.60902256
24	MMP2	matrix metalloproteinase 2	57	137.25769	0.6022305
25	STAT1	signal transducer and activator of transcription 1	57	122.258095	0.6
26	AR	androgen receptor	56	285.19742	0.6
27	ICAM1	intercellular adhesion molecule 1	56	141.12985	0.5912409
28	IL2	interleukin 2	53	109.959145	0.5869565
29	IGF1R	Insulin-like growth factor 1 receptor	53	99.40225	0.5934066
30	MCL1	MCL1 apoptosis regulator, BCL2 family member	52	73.09796	0.5869565
31	PIK3R1	phosphoinositide-3-kinase regulatory subunit 1	52	62.69129	0.57857144
32	JAK2	Janus kinase 2	52	88.90997	0.5890909
33	GSK3B	glycogen synthase kinase 3 beta	51	211.39423	0.5869565
34	RELA	RELA proto-oncogene, NF-kB subunit	51	66.774574	0.5890909
35	KDR	kinase insert domain receptor	51	63.800278	0.5890909
36	MAPK14	mitogen-activated protein kinase 14	49	76.58662	0.5827338
37	ITGB1	integrin subunit beta 1	48	85.17288	0.58064514
38	MAP2K1	mitogen-activated protein kinase kinase 1	47	47.435524	0.57857144
39	PTPN11	protein tyrosine phosphatase non-receptor type 11	47	92.05934	0.5744681
40	NR3C1	nuclear receptor subfamily 3 group C member 1	46	184.64311	0.57857144
41	KIT	KIT proto-oncogene, receptor tyrosine kinase	46	54.70788	0.5724382
42	HDAC1	histone deacetylase 1	46	59.483765	0.57651246
43	PPARA	peroxisome proliferator activated receptor alpha	45	297.67352	0.57651246
44	CCNB1	cyclin B1	44	48.724422	0.56842107
45	PTK2	protein tyrosine kinase 2	44	58.724648	0.5644599
46	MET	MET proto-oncogene, receptor tyrosine kinase	44	76.89858	0.5724382
47	CDK2	cyclin dependent kinase 2	43	46.256893	0.57042253
48	ITGB3	integrin subunit beta 3	43	91.44984	0.56842107
49	SERPINE1	serpin family E member 1	43	93.879036	0.57042253
50	TERT	telomerase reverse transcriptase	42	34.67727	0.56643355
51	PARP1	poly(ADP-ribose) polymerase 1	41	35.284046	0.5586207
52	CDK1	cyclin dependent kinase 1	40	57.485664	0.552901
53	PRKCA	protein kinase C alpha	39	52.762524	0.5625
54	CCNA2	cyclin A2	39	30.931059	0.552901
55	PLG	plasminogen	39	94.049126	0.5625
56	CDK6	cyclin dependent kinase 6	38	26.263622	0.54545456
57	RAF1	Raf-1 proto-oncogene, serine/threonine kinase	38	45.22054	0.556701
58	CHEK1	checkpoint kinase 1	37	33.451557	0.54362416
59	PTPN1	protein tyrosine phosphatase non-receptor type 1	37	54.673954	0.5586207
60	DNMT1	DNA methyltransferase 1	36	44.08532	0.55479455
61	LCK	LCK proto-oncogene, Src family tyrosine kinase	36	46.40462	0.54545456
62	REN	renin	35	106.953285	0.556701
63	PLAU	plasminogen activator, urokinase	35	35.150433	0.552901
64	MMP14	matrix metalloproteinase 14	35	65.272804	0.54545456
65	ESR2	estrogen receptor 2	34	121.78707	0.552901
66	MMP3	matrix metalloproteinase 3	33	28.176418	0.54545456
67	CYP19A1	cytochrome P450 family 19 subfamily A member 1	33	187.62192	0.5510204
68	FLT1	fms related receptor tyrosine kinase 1	33	20.362734	0.5472973

(continued on next page)

Table 4 (continued)

Sr. No.	Genes	Description	Degree	Betweenness	Closeness
69	MMP1	matrix metalloproteinase 1	33	31.671835	0.54915255
70	CHEK2	checkpoint kinase 2	33	38.43983	0.54
71	IGFBP3	insulin like growth factor binding protein 3	32	35.552975	0.54915255
72	ITGAV	integrin subunit alpha V	32	13.124252	0.53289473
73	AHR	aryl hydrocarbon receptor	32	58.796528	0.5510204
74	ABCB1	ATP binding cassette subfamily B member 1	32	153.66301	0.54915255
75	PIK3CG	phosphatidylinositol-4,5-bisphosphate 3-kinase catalytic subunit gamma	32	44.75094	0.53114754
76	SYK	spleen associated tyrosine kinase	31	21.92211	0.538206
77	FGFR1	fibroblast growth factor receptor 1	30	6.8657784	0.5346535
78	CYP3A4	cytochrome P450 family 3 subfamily A member 4	30	185.59036	0.54545456
79	CSF1R	colony stimulating factor 1 receptor	30	22.607122	0.52427185
80	NOS2	nitric oxide synthase 2	29	34.59135	0.53114754
81	ABCG2	ATP binding cassette subfamily G member 2 (Junior blood group)	29	118.69878	0.54
82	CDC25A	cell division cycle 25A	29	33.50356	0.51757187
83	INSR	insulin receptor	29	60.00144	0.54
84	MAPT	microtubule associated protein tau	29	204.23656	0.53289473
85	PLK1	polo like kinase 1	29	20.214935	0.5225806
86	HDAC6	histone deacetylase 6	28	10.963182	0.5346535
87	IDH1	isocitrate dehydrogenase (NADP(+)) 1	28	23.280338	0.52427185
88	TOP2A	DNA topoisomerase II alpha	28	28.069458	0.5192308
89	MPO	myeloperoxidase	28	80.9755	0.5294118
90	AURKA	aurora kinase A	27	14.356633	0.5225806
91	TYMS	thymidylate synthetase	27	88.24776	0.52427185
92	FGF1	fibroblast growth factor 1	26	6.721042	0.53114754
93	VDR	vitamin D receptor	25	27.82825	0.53642386
94	ADAM17	ADAM metalloproteinase domain 17	25	56.23033	0.5192308
95	PRKCB	Protein kinase C beta type	25	42.01173	0.52597404
96	ALK	ALK receptor tyrosine kinase	25	49.2866	0.5209003
97	CYP1A1	cytochrome P450 family 1 subfamily A member 1	25	82.161644	0.53114754
98	CTSB	cathepsin B	25	49.136707	0.52427185
99	CA9	carbonic anhydrase 9	24	46.12754	0.52597404
100	FASN	fatty acid synthase	24	101.87332	0.5346535
101	MMP13	matrix metalloproteinase 13	23	15.944833	0.5225806
102	BRD4	bromodomain containing 4	23	3.9174032	0.5209003
103	PLA2G4A	phospholipase A2 group IVA	23	65.94997	0.52427185
104	NQO1	NAD(P)H quinone dehydrogenase 1	21	41.497147	0.52597404
105	CYP1A2	cytochrome P450 family 1 subfamily A member 2	20	72.98112	0.48795182
106	AGTR1	angiotensin II receptor type 1	20	5.024238	0.51592356
107	CYP1B1	cytochrome P450 family 1 subfamily B member 1	19	44.333103	0.50625
108	BCL2A1	BCL2 related protein A1	19	31.680834	0.51428574
109	COMT	catechol-O-methyltransferase	19	94.680855	0.47928995
110	MDM4	MDM4 regulator of p53	19	4.836352	0.509434
111	PLAT	plasminogen activator, tissue type	18	4.8013134	0.489426
112	ADRB2	adrenoceptor beta 2	18	65.92537	0.51592356
113	BCL2	BCL2 apoptosis regulator	18	18.780884	0.509434
114	APEX1	apurinic/aprimidinic endodeoxyribonuclease 1	18	4.600881	0.50625
115	CXCR2	C-X-C motif chemokine receptor 2	17	1.1007255	0.5031056
116	CCR5	C-C motif chemokine receptor 5	17	12.805787	0.501548
117	F2R	coagulation factor II thrombin receptor	17	10.679118	0.49846154
118	IDO1	indoleamine 2,3-dioxygenase 1	15	25.499634	0.49541286
119	AKR1B1	aldo-keto reductase family 1 member B	15	27.681248	0.509434
120	FUT4	fucosyltransferase 4	15	6.3393993	0.4909091
121	CTSL	cathepsin L	14	325.0352	0.48358208
122	PTGS1	prostaglandin-endoperoxide synthase 1	14	43.242702	0.5
123	CYP2C19	cytochrome P450 family 2 subfamily C member 19	14	26.22645	0.4414169
124	CYP17A1	cytochrome P450 family 17 subfamily A member 1	14	13.776432	0.4668588
125	SHBG	sex hormone binding globulin	14	22.489359	0.48795182
126	PRKCE	protein kinase C epsilon	14	3.5172348	0.4924012
127	EGLN1	egl-9 family hypoxia inducible factor 1	13	6.8312836	0.4924012
128	CXCR3	C-X-C motif chemokine receptor 3	12	1.4342908	0.48502994
129	IGFBP2	insulin like growth factor binding protein 2	12	3.5757694	0.49846154
130	SREBF2	sterol regulatory element binding transcription factor 2	12	2.2590811	0.501548
131	HSD17B1	hydroxysteroid 17-beta dehydrogenase 1	12	8.709829	0.44751382
132	RARB	retinoic acid receptor beta	11	3.3470821	0.48502994
133	NEK2	NIMA related kinase 2	11	0	0.46022728
134	SCD	stearoyl-CoA desaturase	11	24.99222	0.489426
135	ESRRA	estrogen related receptor alpha	11	0.6026418	0.50625
136	PLA2G2A	phospholipase A2 group IIA	11	11.414219	0.489426
137	EDNRA	endothelin receptor type A	11	0.4446036	0.49390244

(continued on next page)

Table 4 (continued)

Sr. No.	Genes	Description	Degree	Betweenness	Closeness
138	UGT2B7	UDP glucuronosyltransferase family 2 member B7	10	2.4204574	0.38942307
139	ESRRB	estrogen related receptor beta	10	5.756692	0.49390244
140	ABCC1	ATP binding cassette subfamily C member 1	10	2.972476	0.501548
141	IGFBP1	insulin like growth factor binding protein 1	10	3.163492	0.49390244
142	STS	steroid sulfatase	9	1.0129288	0.4402174
143	PSEN2	presenilin 2	9	14.722665	0.45
144	MGLL	monoglyceride lipase	9	25.517069	0.45
145	PKD1	pyruvate dehydrogenase kinase 1	9	2.0007868	0.48502994
146	ODC1	ornithine decarboxylase 1	8	2.3115442	0.48502994
147	DAPK1	death associated protein kinase 1	7	1.1552964	0.47928995
148	ACHE	acetylcholinesterase (Cartwright blood group)	7	8.516614	0.48358208
149	IGFBP5	insulin like growth factor binding protein 5	7	0.598472	0.4764706
150	PDE4D	phosphodiesterase 4D	6	1.3218812	0.46285716
151	BCHE	butyrylcholinesterase	6	11.999971	0.45
152	PIM1	Pim-1 proto-oncogene, serine/threonine kinase	6	0.24066626	0.46153846
153	CRHR1	corticotropin releasing hormone receptor 1	6	2.980681	0.44505495
154	XDH	xanthine dehydrogenase	6	10.574237	0.45251396
155	NCSTN	nicastatin	5	0.3789813	0.43548387
156	PTPRF	protein tyrosine phosphatase receptor type F	5	0.102380954	0.44383562
157	FABP3	fatty acid binding protein 3	5	2.1826377	0.40703517
158	PABPC1	poly(A) binding protein cytoplasmic 1	4	0.47563234	0.4297082
159	CNR2	cannabinoid receptor 2	4	322.72867	0.43431637
160	HPGD	15-hydroxyprostaglandin dehydrogenase	3	0	0.41860464
161	CA12	carbonic anhydrase 12	3	0	0.43665767
162	MTNR1A	melatonin receptor 1A	1	0	0.30337077
163	HPSE	heparanase	1	0	0.3266129

beneficial to analyse the formation and disruption of H-bonds over time during simulation. Intermolecular hydrogen bonds within the docked EGFR-lanaroflavone and CTNNB1-sequoiaflavone complexes play a crucial role in maintaining the stability of the protein-ligand interactions. Specifically, the EGFR-lanaroflavone complex was stabilized by two hydrogen bonds (see Figure-13C), while the CTNNB1-sequoiaflavone complex exhibited three hydrogen bonds (see Figure-14C). Molecular stability can also be evaluated through the compactness of protein molecules, quantified by the Radius of Gyration (Rg) in molecular dynamics (MD) simulations. Rg serves as a measure of the overall size and shape of a protein structure, reflecting its tertiary structure. In this study, Rg values were employed to assess the compactness of EGFR and CTNNB1 following binding with lanaroflavone and sequoiaflavone. The EGFR-lanaroflavone complex (Figure-13D) and CTNNB1-sequoiaflavone complex (Figure-14D) displayed average Rg values of 2.0 nm and 3.11 nm, respectively. The Rg plots illustrate that both protein-ligand complexes maintained a compact structure throughout the simulation, with no significant alterations observed. SASA (Solvent Accessible Surface Area) provides insights into the portion of a protein molecule's surface accessible to its surrounding solvent molecules. In MD analysis, SASA analysis serves as a valuable tool for investigating protein folding, unfolding and structural stability. Analysis of SASA values during the simulations revealed no significant peaks, suggesting that the binding of lanaroflavone and sequoiaflavone did not markedly influence the folding behaviour of EGFR and CTNNB1. The EGFR-lanaroflavone complex (Figure-13E) exhibited an average SASA value of 154.81 nm², while the CTNNB1-sequoiaflavone complex (Figure-14E) displayed an average SASA value of 270.55 nm². These results indicate that EGFR and CTNNB1 maintained stability in the presence of lanaroflavone and sequoiaflavone, as reflected by their SASA values.

3.7. PCA and FELs analyses

The conformational dynamics of proteins are crucial for their biological functions and exploring these dynamics provides insights into their stability and activity during simulations. Principal Component Analysis (PCA) has proven to be a valuable tool for investigating the atomic motions within proteins and visualizing their conformational changes. In this study, PCA was conducted on all C α atoms of the EGFR-lanaroflavone and CTNNB1-sequoiaflavone complexes, focusing on the first two principal components (PC1 and PC2) to project their conformational states onto a two-dimensional subspace. Figs. 15A and 16A depict the resulting projections, where densely populated regions represent stable protein conformations. The projection of EGFR-lanaroflavone onto PC1 and PC2 revealed variance contributions of -6 and 6, respectively (Fig. 15B), while for CTNNB1-sequoiaflavone, the contributions were -12 and 18 (Fig. 16B). These findings highlight the stability and variability of protein conformations in the ligand-bound states, as captured by PCA.

Free Energy Landscapes (FELs) offer valuable insights into the aging of protein folding mechanisms and the impact of ligand binding on protein structure and stability. In this study, FELs were generated to elucidate the global minima and conformational landscape of the EGFR-lanaroflavone and CTNNB1-sequoiaflavone complexes. The FEL plots, represented in Figs. 17 and 18, highlighted regions of lower energy (depicted in deeper blue), indicating stable protein conformations near the global minimum. Both EGFR-lanaroflavone and CTNNB1-sequoiaflavone complexes exhibited a single global minimum confined within a large basin. This analysis suggested that the binding of lanaroflavone and sequoiaflavone resulted in a stable conformational state for both EGFR and CTNNB1. These findings provide further support for the potential of lanaroflavone and sequoiaflavone as therapeutic agents targeting

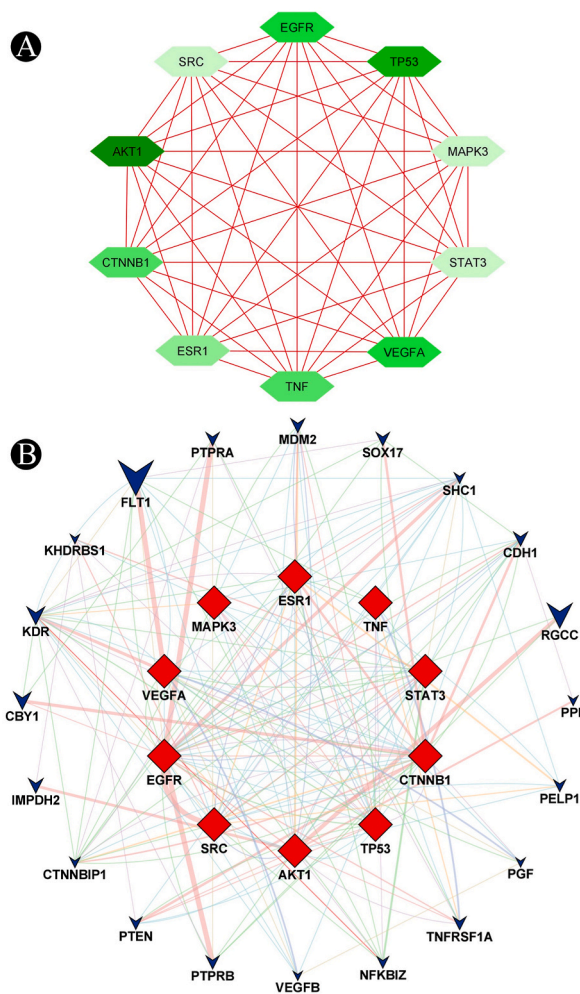


Fig. 5. (A). Identified hub-genes in a PPI network obtained from common target genes of phytochemical constituents of *S. bryopteris* and breast cancer, (B). Network of hub-genes against breast cancer analyzed by GeneMANIA. Functional association of targets was analyzed and connecting lines with different colors represent different correlations. Genes associated with query genes were indicated by nodes on the outer ring. The genes shown in the inner ring were used as search terms to find relevant information. (For interpretation of the references to color in this figure legend, the reader is referred to the Web version of this article.)

EGFR and CTNNB1, given their stable binding interactions observed throughout the simulation.

3.8. MMPBSA binding free energy

The binding free energy of the EGFR-lanaroflavone and CTNNB1-sequoiaflavone complexes was estimated using MD trajectory analysis. The results revealed significant binding affinities for lanaroflavone and sequoiaflavone with EGFR and CTNNB1, respectively, with values of -114.185 ± 18.561 kJ/mol and -87.988 ± 5.197 kJ/mol. The MMPBSA analysis further corroborated these findings, supporting the observation of appreciable binding affinity between lanaroflavone and sequoiaflavone with EGFR and CTNNB1.

3.9. Extract preparation and anticancer activity of *S. bryopteris* crude extract

Prior to the preparation of the final plant extract, *S. bryopteris* powder was extracted using a range of solvent systems with varying polarity through the maceration technique to obtain different bioactive compounds. The quantity of bioactive compounds extracted in each solvent was assessed by calculating the percentage yield (%). The highest yield was obtained with 85 % ethanol and therefore, the final extract used for various biological activities was prepared in this solvent. *S. bryopteris* crude extract was tested for anticancer activity against MCF-7 breast cancer cells using the MTT assay. A time- and dose-dependent inhibition of breast cancer cell viability was observed with *S. bryopteris* crude extract. A higher concentration of the crude extract results in a lower viability of breast cancer cells. *S. bryopteris* crude extract had an IC_{50} value of 78.34 μ g/mL against MCF-7 breast cancer cells, indicating that this concentration

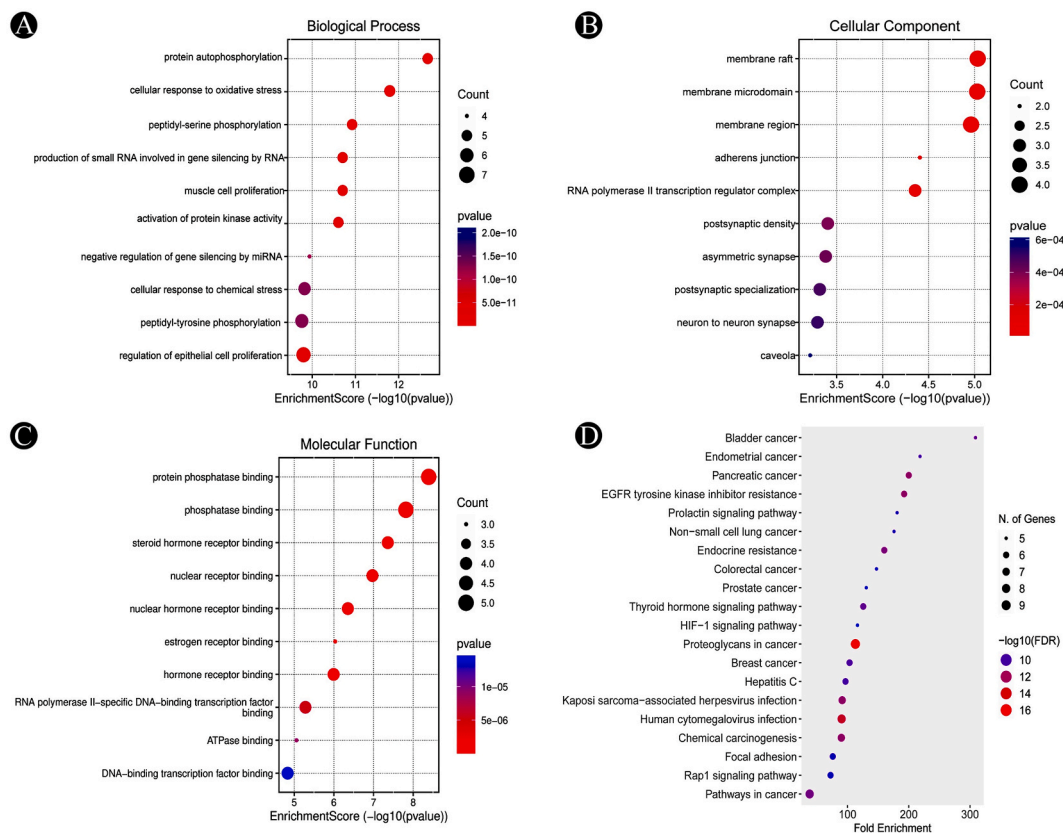


Fig. 6. KEGG pathway and GO enrichment analyses of identified hub-target proteins (p -value ≤ 0.05). (A). The biological processes (top 10), (B). The cellular components (top 10), (C). The molecular functions (top 10), (D). The KEGG pathways (top 20). The p -values for each term are shown by the colors, with darker colors indicating lower p -values. The number of genes associated with each term are indicated by the dot sizes, with larger dots representing more genes. (For interpretation of the references to color in this figure legend, the reader is referred to the Web version of this article.)

of *S. bryopteris* crude extract reduced the survival rate of breast cancer cells by 50 % (Figure-19A & B).

3.10. Inhibition of cell migration by *S. bryopteris* crude extract

Cancer metastasis occurs when cancer cells spread from the primary site to other parts of the body via cell migration. MCF-7 cells were tested for cell migration by scratch assays using crude extract of *S. bryopteris*. A gap was created in a monolayer of cells and an assay was performed to determine if the cells were able to fill the gap in the presence or absence of a crude extract of *S. bryopteris*. Figure-20 represents the results of scratch assay. In comparison with the control group, crude extract of *S. bryopteris* significantly reduced cell migration. After 19 and 44 h of scratching, MCF-7 cancer cells in the control group gradually closed the gap, whereas the IC_{50} concentration of *S. bryopteris* crude extract prevented the gap from closing. According to these results, *S. bryopteris* crude extract impairs cell migration, which may contribute to its anti-metastatic properties.

3.11. Inhibition of cell invasion by *S. bryopteris* crude extract

The effect of *S. bryopteris* crude extract on cell invasion was tested by Transwell chamber assays on human breast cancer MCF-7 cells. Transwell chambers were used to determine whether cells could pass through a Matrigel-coated membrane mimicking extracellular matrix in the presence or absence of crude extract from *S. bryopteris*. Figure-20 displays the results of cell invasion assay. The results revealed that *S. bryopteris* crude extract significantly impaired the invasion of cells compared to the control group. The IC_{50} concentration of *S. bryopteris* crude extract reduced the number of invading MCF-7 cells. These results suggest that *S. bryopteris* crude extract has an anti-invasive effect by blocking cell invasion.

4. Discussion

Cancer is a complex and heterogeneous disease that involves the dysregulation of multiple cellular processes and pathways [3,4].

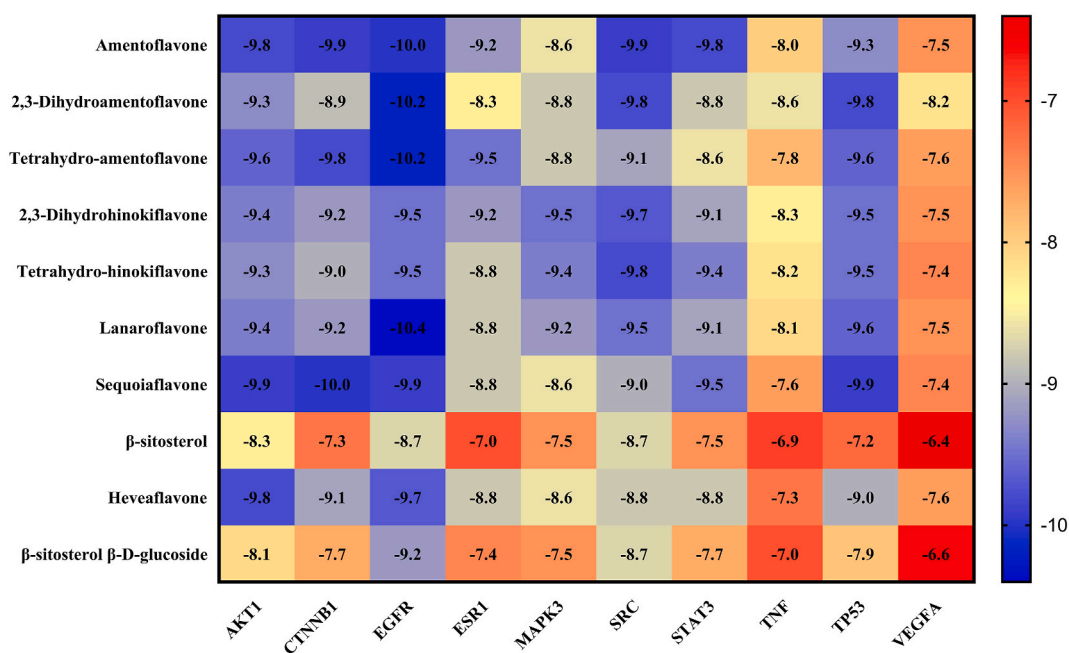


Fig. 7. Binding affinity of the top-rated pose of a protein-ligand complex obtained after molecular docking analysis.

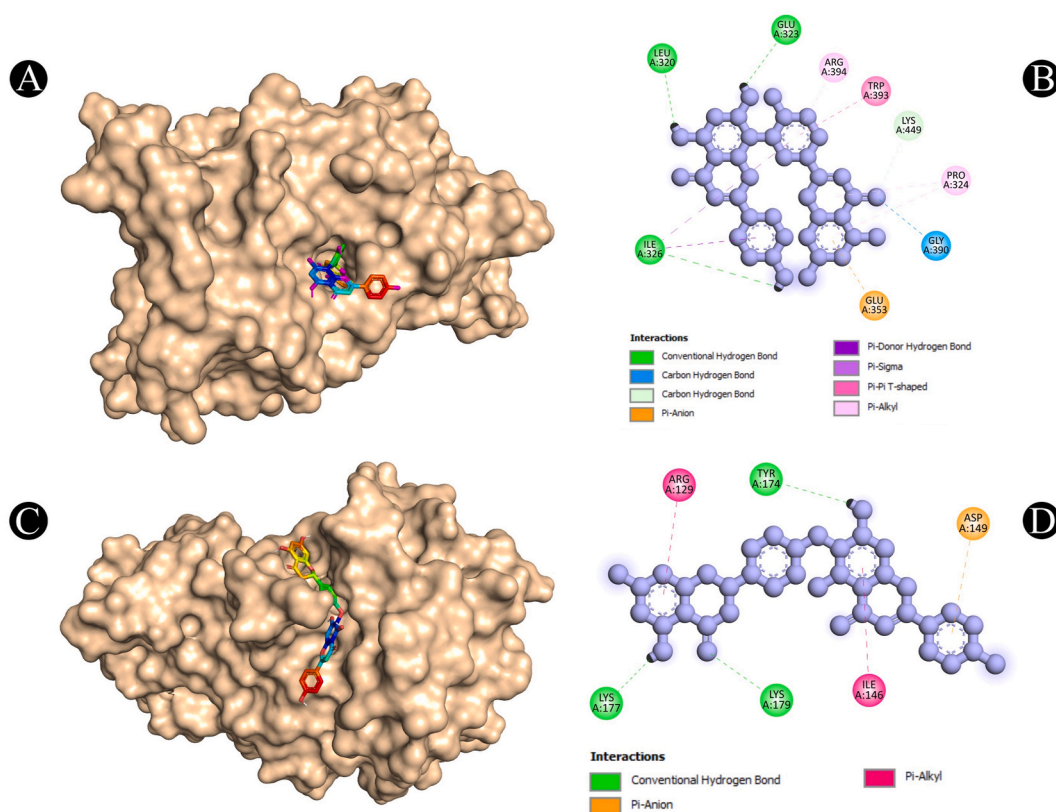


Fig. 8. (A & B). The result of the molecular docking study shows how amentoflavone binds to ESR1, (C & D). The result of the molecular docking study shows how 2,3-dihydrohinokiflavone binds to MAPK3 protein.

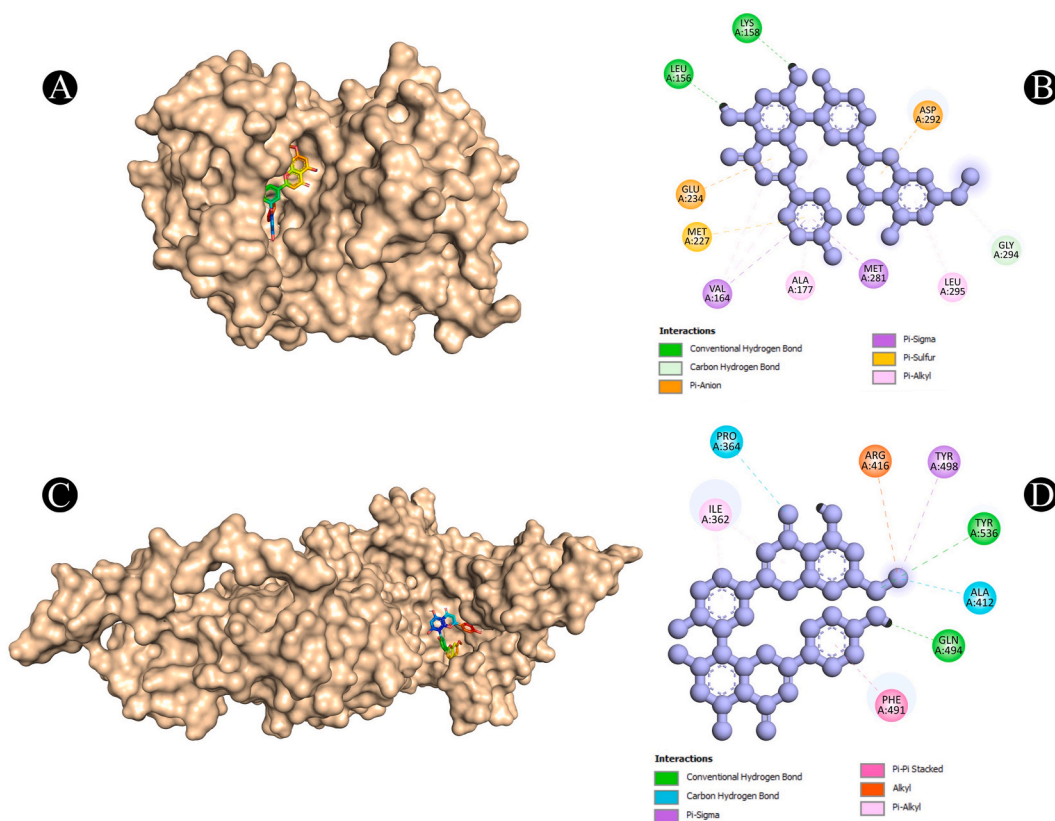


Fig. 9. (A & B). The result of the molecular docking study shows how sequoiaflavone binds to AKT1, (C & D). The result of the molecular docking study shows how sequoiaflavone binds to CTNNB1.

Understanding the molecular mechanisms of cancer initiation, progression and response to therapy is essential for developing effective strategies for prevention, diagnosis and treatment [58]. Biomolecular structure and/or dynamics (BSD) is an interdisciplinary field that applies computational and experimental methods to study the structure, function and interactions of biomolecules involved in cancer [59–61]. BSD can provide insights into the molecular basis of cancer at different levels of complexity, from genes and proteins to pathways and networks. BSD has contributed to various aspects of cancer research, such as identifying novel biomarkers, targets and drugs; elucidating the effects of mutations, post-translational modifications and epigenetic changes; exploring the mechanisms of drug resistance and sensitivity and designing rational drug combinations [62–64]. The structure of biomolecules, such as proteins plays a crucial role in cancer research. Proteins are involved in various cellular processes, including cell signaling, DNA replication and cell division [65,66]. Alterations in protein structure can lead to dysregulated cellular functions, contributing to cancer development. Therefore, understanding the three-dimensional structure of proteins and their interactions with other molecules is essential for identifying potential targets for cancer therapies [67,68].

Natural phytochemical constituents derived from the plants have been important for drug discovery for centuries [10]. Different types of phytochemical constituents are recognised as valuable sources of pharmacologically bioactive compounds and therefore their application in drug development cannot be ignored [8,9]. Plants are able to synthesize diverse range of secondary metabolites including alkaloids, flavonoids, terpenoids, phenolics, saponins etc. which possess vast and diverse chemical structures [17,18]. Such chemodiversity of plants attracts the researchers for the findings of their potential application in a variety of diseases. Moreover, natural compounds are considered as safe and less toxic in comparison to synthetic chemicals. Therefore, natural compounds are the first choice as a drug candidate [69,70].

Drug discovery and development are costly and lengthy processes. It can take more than a decade and high cost to bring a new drug to market. During the process of drug development, a failure rate in drug development is high as many drug compounds failing in clinical trials [71]. This is often due to unexpected safety issues or lack of efficacy. Identifying and validating drug targets remains a significant challenge. For a successful drug development, understanding of the complexity of diseases is an essential. The rise in a problem of drug resistance specially in antibiotics and anticancer drugs creates a major concern at the present time in a medical sector [72–74]. Such type of limitations during the drug discovery process can be sort out with the help of network pharmacology approach. Network pharmacology approach focuses on the interactions of multiple genes, proteins, and pathways which are involved in a particular diseases condition instead of on a single drug-target interactions. Hence, the development of highly effective drugs with lower side effects is possible via this computational approach. It helps to identify key nodes in disease-related networks, facilitating

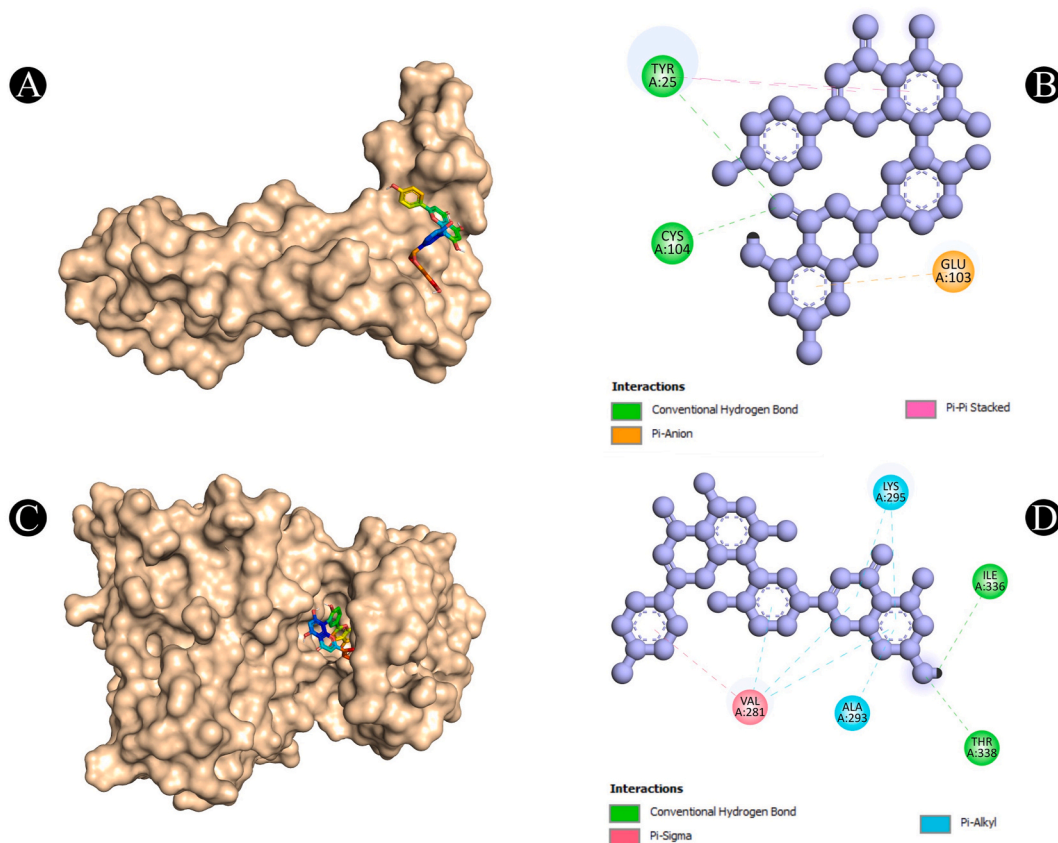


Fig. 10. (A & B). The result of the molecular docking study shows how 2,3-dihydroamentoflavone binds to VEGFA, (C & D). The result of the molecular docking study shows how amentoflavone binds to SRC.

target identification and validation [3,28,30]. By analyzing existing drug-target networks, network pharmacology can identify new therapeutic uses for existing drugs, speeding up the drug development process and reducing costs [75].

From centuries, *S. bryopteris* is utilized as a medicine against different types of ailments including cancer [76]. However, the molecular mechanisms and targets involved in its anti-cancer activity are not very well known. Therefore, the present study was carried out via network pharmacology-based analysis to identify the potential cancer-related targets and pathways of *S. bryopteris* and its phytochemical constituents. As an additional step, validation of the network pharmacology predictions on breast cancer cell lines has been performed to test the cytotoxicity and anti-metastasis activity *in-vitro*. The phytochemical data of *S. bryopteris* from various databases and literature sources was collected and screened them for drug-likeness and oral bioavailability. Total 10 phytochemicals were obtained that met the criteria and used them as input for network pharmacology analysis. The compound-target network was constructed after retrieving the targets of the phytochemicals constituents of *S. bryopteris* from SwissTargetPrediction database. Then, the retrieved targets were mapped to the breast cancer related genes obtained from OMIM, DisGeNET and GeneCards database in which total 163 common targets were obtained. The functional enrichment analysis of the obtained common targets were performed via DAVID database and found that the common targets were involved with various biological processes, cellular components, molecular functions and pathways which are related to breast and other cancers. Some of the enriched terms were EGFR tyrosine kinase inhibitor resistance, prolactin signaling pathway, HIF-1 signaling pathway, Rap1 signaling pathway, pathways in cancer and breast cancer. (see Fig. 12)

In the present study, EGFR, TP53, MAPK3, STAT3, VEGFA, TNF, ESR-1, CTNBN1, AKT-1 and SRC were identified as the top ten targets in the PPI network constructed [77]. EGFR is a well-known target for the treatment of different types of cancer including breast cancer as it is often overexpressed in cancer conditions [78]. It is involved in several important biological processes such as, regulating cell growth, differentiation and survival. It plays an important role in the formation and progression of triple-negative breast cancer and inflammatory breast cancer. It can activate several downstream pathways including MAPK, PI3K/AKT, and STAT3 pathways which are involved in the regulation of cell proliferation, survival, invasion, angiogenesis, and epithelial-mesenchymal transition (EMT) [79]. TP53 is a tumor suppressor gene that encodes p53, a transcription factor that regulates cell cycle, apoptosis, DNA repair, and senescence. TP53 is frequently mutated or deleted in breast cancer, leading to loss of its function and increased tumor growth and resistance to therapy. Restoring p53 activity or targeting its downstream effectors is a promising strategy for breast cancer treatment [80]. MAPK3 is a gene that encodes ERK1, a member of the mitogen-activated protein kinase (MAPK) family that mediates cellular

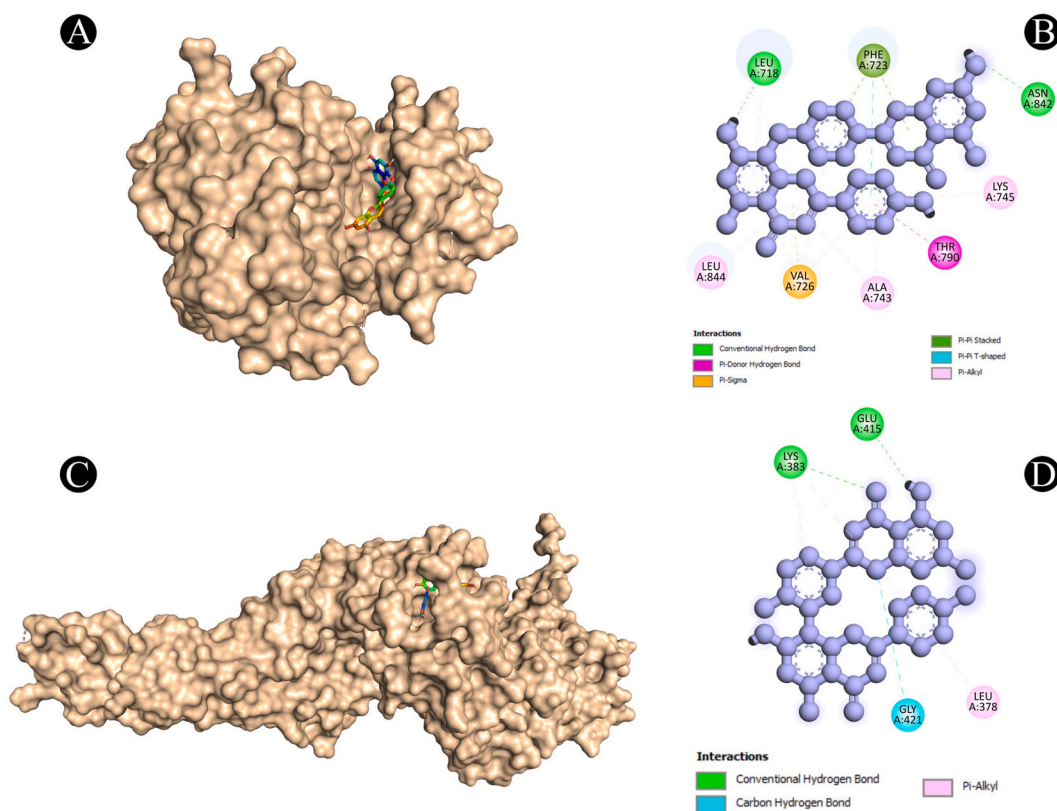


Fig. 11. (A & B). The result of the molecular docking study shows how lanaroflavone binds to EGFR, (C & D). The result of the molecular docking study shows how amentoflavone binds to STAT3.

responses to growth factors, cytokines, and stress stimuli. MAPK3 is often overexpressed or activated in breast cancer, especially in the triple-negative subtype, and promotes tumor proliferation, invasion, angiogenesis, and metastasis. Inhibiting MAPK3 or its upstream regulators (such as RAS and RAF) or downstream targets (such as MYC and ETS) is a potential therapeutic approach for breast cancer [81,82]. STAT3 is a gene that encodes STAT3, a transcription factor that is activated by the JAK/STAT pathway in response to various cytokines and growth factors. STAT3 is constitutively activated in breast cancer, especially in the inflammatory and HER2-positive subtypes, and regulates tumor survival, growth, angiogenesis, inflammation, immune evasion, and chemoresistance. Targeting STAT3 or its upstream activators (such as IL-6 and EGFR) or downstream genes (such as BCL-2 and VEGF) is a promising strategy for breast cancer treatment [83–85].

VEGFA is a gene that encodes vascular endothelial growth factor A (VEGF-A), a key factor that stimulates angiogenesis and lymphangiogenesis by binding to its receptors (VEGFR1 and VEGFR2) on endothelial cells. VEGFA is overexpressed in breast cancer, especially in the hypoxic and HER2-positive subtypes, and promotes tumor growth, invasion, metastasis, and resistance to therapy. Blocking VEGFA or its receptors with antibodies or small molecules is an effective anti-angiogenic therapy for breast cancer [2,86]. TNF is a gene that encodes tumor necrosis factor (TNF), a pro-inflammatory cytokine that induces cell death, inflammation, and immune responses by binding to its receptors (TNFR1 and TNFR2) on various cells. TNF has a dual role in breast cancer: it can inhibit tumor growth by inducing apoptosis and immune activation, or it can promote tumor progression by stimulating angiogenesis, invasion, metastasis, and chemoresistance. Modulating TNF signaling with antagonists or agonists may have therapeutic benefits for breast cancer [87]. ESR1 is a gene that encodes estrogen receptor alpha (ER α), a nuclear hormone receptor that mediates the effects of estrogen on gene expression and cellular functions. ESR1 is expressed in about 70 % of breast cancers, especially in the luminal subtype, and stimulates tumor growth, survival, differentiation, and metastasis. Inhibiting ESR1 or its ligand (estrogen) or coactivators with selective estrogen receptor modulators (SERMs), aromatase inhibitors (AIs), or histone deacetylase inhibitors (HDACIs) is an effective endocrine therapy for breast cancer [88].

CTNNB1 is a gene that encodes β -catenin, a multifunctional protein that acts as a component of the adherens junctions and a mediator of the Wnt/ β -catenin signaling pathway. CTNNB1 is aberrantly activated in breast cancer, especially in the basal-like subtype, and regulates tumor stemness, proliferation, invasion, metastasis, and resistance to therapy. Targeting CTNNB1 or its upstream regulators (such as Wnt ligands and receptors) or downstream targets (such as c-MYC and cyclin D1) is a potential therapeutic approach for breast cancer [89]. AKT1 is a gene that encodes AKT1, a serine/threonine kinase that is activated by the PI3K/AKT/mTOR pathway in response to various growth factors and cytokines. AKT1 is frequently amplified or activated in breast cancer, especially in the HER2-positive and luminal subtypes, and regulates tumor survival, growth, metabolism, angiogenesis,

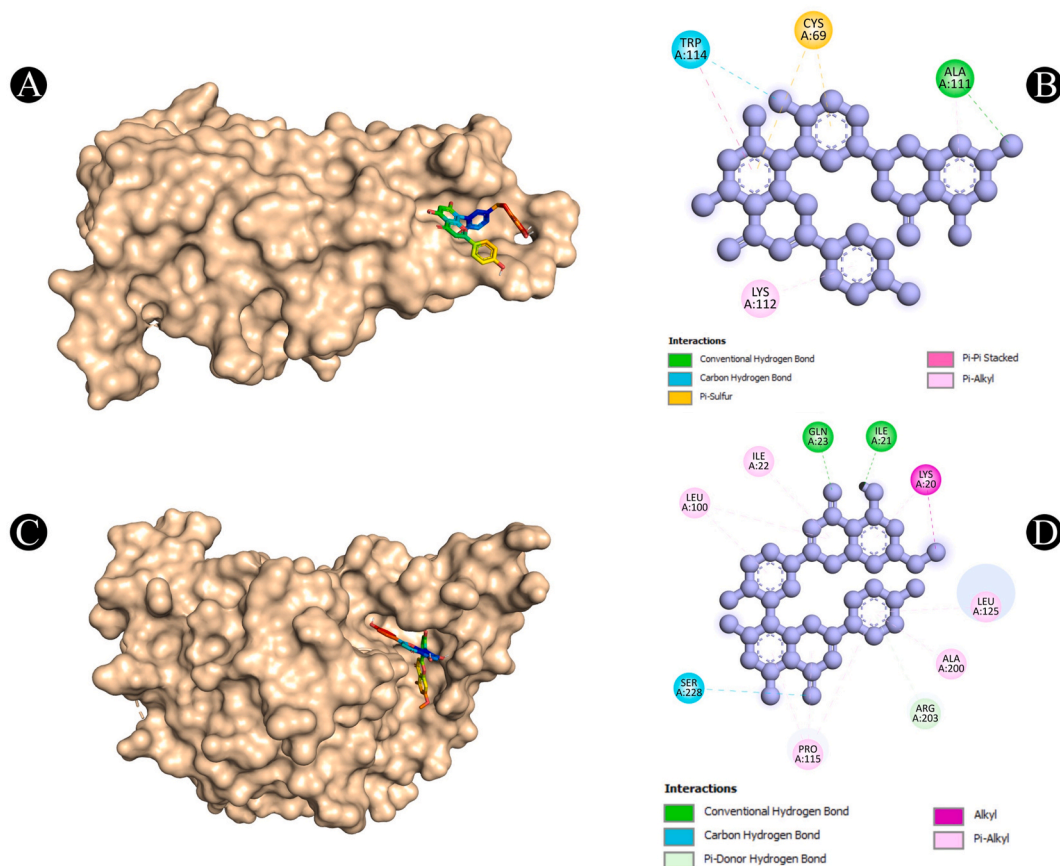


Fig. 12. (A & B). The result of the molecular docking study shows how 2,3-dihydroamentoflavone binds to TNF, (C & D). The result of the molecular docking study shows how sequoiaflavone binds to TP53.

invasion, metastasis, and resistance to therapy. Inhibiting AKT1 or its upstream activators (such as PI3K and PTEN) or downstream effectors (such as mTOR and FOXO) is a promising strategy for breast cancer treatment [90,91]. SRC is a gene that encodes SRC, a non-receptor tyrosine kinase that is involved in various signaling pathways, such as EGFR, HER2, integrin, and focal adhesion kinase (FAK) pathways. SRC is often overexpressed or activated in breast cancer, especially in the basal-like and HER2-positive subtypes, and regulates tumor proliferation, invasion, migration, metastasis, and resistance to therapy. Targeting SRC or its upstream regulators (such as EGFR and HER2) or downstream targets (such as FAK and STAT3) is a potential therapeutic approach for breast cancer [92].

An GO enrichment analysis was used to identify the biological details of the target genes, revealing the main functions of the target genes included in cellular response to oxidative stress, muscle cell proliferation, epithelial cell proliferation regulation, cellular response to chemical stress, phosphorylation of peptidyl-tyrosine, activating protein kinases, and phosphorylation of peptidyl-serine. It is evident from the KEGG pathway enrichment data that the potential targets of this study are strongly associated with cancer-related pathways, such as HIF-1 signaling, prolactin signaling, proteoglycans in cancer, Rap1 signaling pathway, and EGFR tyrosine kinase inhibitor resistance pathway. Based on these findings, phytochemical constituents of *S. bryopteris* might play a role in suppressing breast cancer through the medium of these target proteins and signaling pathways mediated by network pharmacology analysis. It has been reported that Amentoflavone and its derivatives are effective in inhibiting the growth of a variety of cancerous cells. Amentoflavone induces apoptosis in esophageal squamous cell carcinoma (ESCC) cells and modulates cyclin B1 expression [93]. Similarly, Hinokiflavone has been shown to inhibit the proliferation and metastasis of hepatocellular carcinoma (HCC) cells by interfering with the ERK1-2/p38/NFκB signaling pathway and regulating the expression of matrix metalloproteinases (MMPs) and pre-mRNA splicing [94]. Both compounds also have immunomodulatory effects by enhancing the production of cytokines and natural killer cell activity [94]. Thus, targeting proteins which are identified via network pharmacology analysis with Amentoflavone, 2,3-Dihydroamentoflavone, Tetrahydro-amentoflavone, 2,3-Dihydrohinokiflavone, Tetrahydro-hinokiflavone, Lanaroflavone, Sequoiaflavone, β-sitosterol, Heveaflavone, β-sitosterol β-D-glucoside, Heveaflavone, Neocryptomerin and Isocryptomerin can result in reducing the chance of breast cancer in affected individuals.

Further the network pharmacology approach in the present study revealed the potential interactions between the phytochemical constituents of *S. bryopteris* and the breast cancer target proteins, based on the molecular docking analysis. A docking analysis was conducted in order to identify key interactions, binding affinities and potential binding modes of the ligands with their respective

Table 5The residues in the target proteins that interact with the phytochemical constituents of *S. bryopteris* in their best-fitting pose.

Sr. No.	Protein-Compound	Receptor-Ligand	Interaction Type	Distance
1	ESR1	N:UNK1:H - A:GLU323:OE1	Conventional Hydrogen Bond	2.45372
		N:UNK1:H - A:ILE326:O	Conventional Hydrogen Bond	2.66433
		N:UNK1:H - A:LEU320:O	Conventional Hydrogen Bond	2.85556
		A:GLY390:CA - N:UNK1:O	Carbon Hydrogen Bond	3.07032
		A:LYS449:CE - N:UNK1:O	Carbon Hydrogen Bond	3.08588
		A:GLU353:OE2 - N:UNK1	Pi-Anion	3.53146
		A:ILE326:HN - N:UNK1	Pi-Donor Hydrogen Bond	2.47951
		A:ILE326:CD1 - N:UNK1	Pi-Sigma	3.74167
		A:TRP393 - N:UNK1	Pi-Pi T-shaped	4.64658
		N:UNK1 - A:ARG394	Pi-Alkyl	5.26413
		N:UNK1 - A:PRO324	Pi-Alkyl	4.28884
		N:UNK1 - A:PRO324	Pi-Alkyl	3.89793
		N:UNK1 - A:ILE326	Pi-Alkyl	4.45301
		2	MAPK3	A:LYS179:HN - N:UNK1:O
N:UNK1:H - A:LYS177:O	Conventional Hydrogen Bond			2.23626
N:UNK1:H - A:TYR174:OH	Conventional Hydrogen Bond			1.77868
A:ASP149:OD1 - N:UNK1	Pi-Anion			3.39783
N:UNK1 - A:ILE146	Pi-Alkyl			5.4424
N:UNK1 - A:ARG129	Pi-Alkyl			5.34238
3	AKT1	N:UNK1:H - A:LYS158:O	Conventional Hydrogen Bond	2.15827
		N:UNK1:H - A:LEU156:O	Conventional Hydrogen Bond	2.98273
		A:GLY294:CA - N:UNK1:O	Carbon Hydrogen Bond	3.41215
		A:GLU234:OE2 - N:UNK1	Pi-Anion	3.48103
		A:ASP292:OD2 - N:UNK1	Pi-Sigma	3.76488
		A:VAL164:CG1 - N:UNK1	Pi-Sigma	3.80774
		A:MET281:CE - N:UNK1	Pi-Anion	3.86431
		A:MET227:SD - N:UNK1	Pi-Alkyl	4.82711
		N:UNK1 - A:VAL164	Pi-Alkyl	4.93972
		N:UNK1 - A:VAL164	Pi-Alkyl	5.39322
		N:UNK1 - A:LEU295	Pi-Alkyl	5.49262
4	CTNNB1	N:UNK1 - A:ALA177	Pi-Sulfur	5.8876
		A:TYR536:HH - N:UNK1:O	Conventional Hydrogen Bond	2.42875
		N:UNK1:H - A:GLN494:OE1	Conventional Hydrogen Bond	2.16781
		A:PRO364:CD - N:UNK1:O	Carbon Hydrogen Bond	3.72295
		N:UNK1:C - A:ALA412:O	Carbon Hydrogen Bond	3.74538
		N:UNK1:C - A:TYR498	Pi-Sigma	3.92109
		A:PHE491 - N:UNK1	Pi-Pi Stacked	3.76492
		N:UNK1:C - A:ARG416	Alkyl	3.94769
		N:UNK1 - A:ILE362	Pi-Alkyl	5.29403
		N:UNK1 - A:ILE362	Pi-Alkyl	4.96493
5	VEGFA	A:TYR25:HH - N:UNK1:O	Conventional Hydrogen Bond	2.21826
		A:CYS104:HN - N:UNK1:O	Conventional Hydrogen Bond	2.32063
		A:GLU103:OE1 - N:UNK1	Pi-Anion	3.75612
		A:TYR25 - N:UNK1	Pi-Pi Stacked	3.80081
6	SRC	A:TYR25 - N:UNK1	Pi-Pi Stacked	3.90359
		A:THR338:HN - N:UNK1:O	Conventional Hydrogen Bond	2.63427
		N:UNK1:H - A:ILE336:O	Conventional Hydrogen Bond	2.02244
		A:VAL281:CG2 - N:UNK1	Pi-Sigma	3.34011
		N:UNK1 - A:VAL281	Pi-Alkyl	4.39825
		N:UNK1 - A:VAL281	Pi-Alkyl	4.41946
		N:UNK1 - A:LYS295	Pi-Alkyl	5.13809
		N:UNK1 - A:VAL281	Pi-Alkyl	5.24847
7	EGFR	N:UNK1 - A:ALA293	Pi-Alkyl	5.01396
		N:UNK1 - A:LYS295	Pi-Alkyl	4.0899
		N:UNK1:H - A:ASN842:OD1	Conventional Hydrogen Bond	2.32638
		N:UNK1:H - A:LEU718:O	Conventional Hydrogen Bond	1.97542
		A:THR790:OG1 - N:UNK1	Pi-Donor Hydrogen Bond	4.1917
		A:VAL726:CG1 - N:UNK1	Pi-Sigma	3.90614
		A:PHE723 - N:UNK1	Pi-Pi Stacked	3.74847
		A:PHE723 - N:UNK1	Pi-Pi Stacked	5.29324
		A:PHE723 - N:UNK1	Pi-Pi T-shaped	5.39063
		N:UNK1 - A:ALA743	Pi-Alkyl	4.88763
		N:UNK1 - A:LEU844	Pi-Alkyl	5.42608
		N:UNK1 - A:LEU718	Pi-Alkyl	4.6556
		N:UNK1 - A:VAL726	Pi-Alkyl	4.75011
N:UNK1 - A:VAL726	Pi-Alkyl	5.35282		
N:UNK1 - A:VAL726	Pi-Alkyl	4.52976		
N:UNK1 - A:ALA743	Pi-Alkyl	4.55853		

(continued on next page)

Table 5 (continued)

Sr. No.	Protein-Compound	Receptor-Ligand	Interaction Type	Distance
8	STAT3	N:UNK1 - A:LYS745	Pi-Alkyl	4.3685
		A:LYS383:HN - N:UNK1:O	Conventional Hydrogen Bond	2.44327
		N:UNK1:H - A:GLU415:OE2	Conventional Hydrogen Bond	2.4635
		A:GLY421:CA - N:UNK1:O	Carbon Hydrogen Bond	3.31331
		N:UNK1 - A:LYS383	Pi-Alkyl	5.0554
9	TNF	N:UNK1 - A:LEU378	Pi-Alkyl	4.91194
		N:UNK1 - A:LYS383	Pi-Alkyl	4.79607
		A:ALA111:HN - N:UNK1:O	Conventional Hydrogen Bond	2.8184
		A:TRP114:CD1 - N:UNK1:O	Carbon Hydrogen Bond	3.19619
		A:CYS69:SG - N:UNK1	Pi-Sulfur	3.92223
10	TP53	A:CYS69:SG - N:UNK1	Pi-Sulfur	5.76024
		A:TRP114 - N:UNK1	Pi-Pi Stacked	5.40202
		N:UNK1 - A:LYS112	Pi-Alkyl	4.0237
		N:UNK1 - A:ALA111	Pi-Alkyl	5.1857
		A:GLN23:HN - N:UNK1:O	Conventional Hydrogen Bond	2.17542
		N:UNK1:H - A:ILE21:O	Conventional Hydrogen Bond	1.98409
		A:SER228:CB - N:UNK1:O	Carbon Hydrogen Bond	3.17627
		A:ARG203:NE - N:UNK1	Pi-Donor Hydrogen Bond	3.30327
		N:UNK1:C - A:LYS20	Alkyl	4.69264
		N:UNK1 - A:PRO115	Pi-Alkyl	3.83854
		N:UNK1 - A:PRO115	Pi-Alkyl	5.20647
		N:UNK1 - A:LEU100	Pi-Alkyl	5.45672
		N:UNK1 - A:ILE22	Pi-Alkyl	5.23874
		N:UNK1 - A:LEU100	Pi-Alkyl	5.43845
		N:UNK1 - A:LYS20	Pi-Alkyl	5.23021
N:UNK1 - A:PRO115	Pi-Alkyl	4.34344		
N:UNK1 - A:LEU125	Pi-Alkyl	5.30129		
N:UNK1 - A:ALA200	Pi-Alkyl	4.47672		
N:UNK1 - A:ARG203	Pi-Alkyl	4.5321		

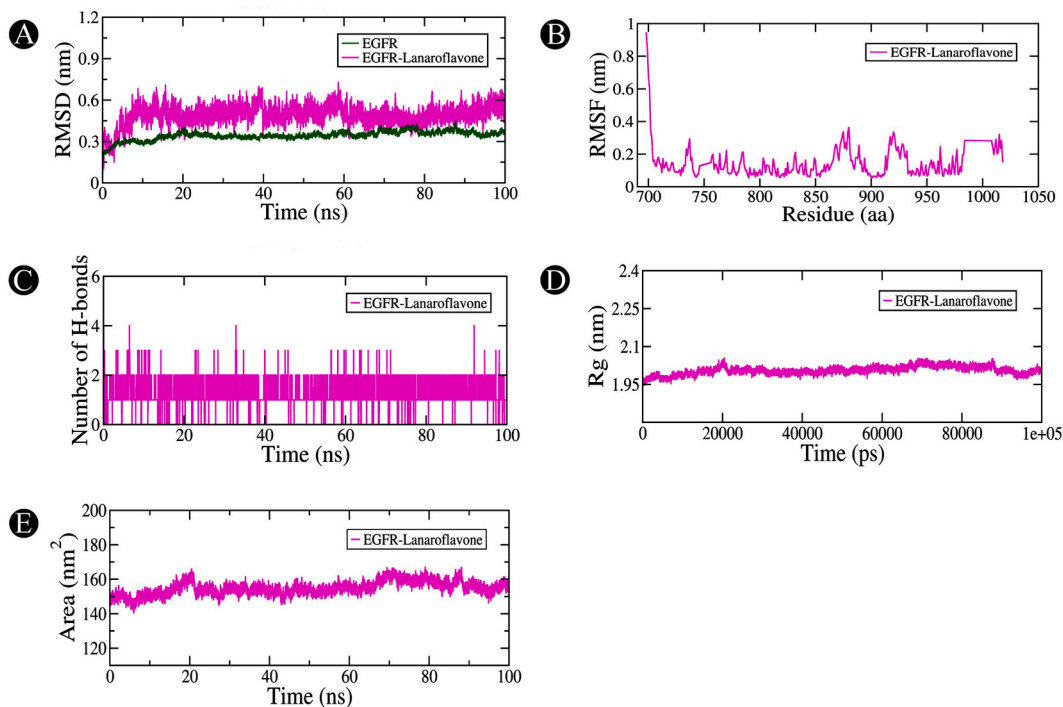


Fig. 13. The molecular dynamics simulation analysis of EGFR protein and lanaroflavone molecule over time. Molecular dynamics of EGFR and its binding with diadzein. (A). RMSD analysis of EGFR with and without lanaroflavone binding, (B). RMSF analysis of EGFR-lanaroflavone complex, (C). EGFR-lanaroflavone complex intermolecular H-bond time evolution within 0.35 nm, (D). The Rg distribution of EGFR-lanaroflavone complex, (E). SASA plot analysis of EGFR-lanaroflavone complex.

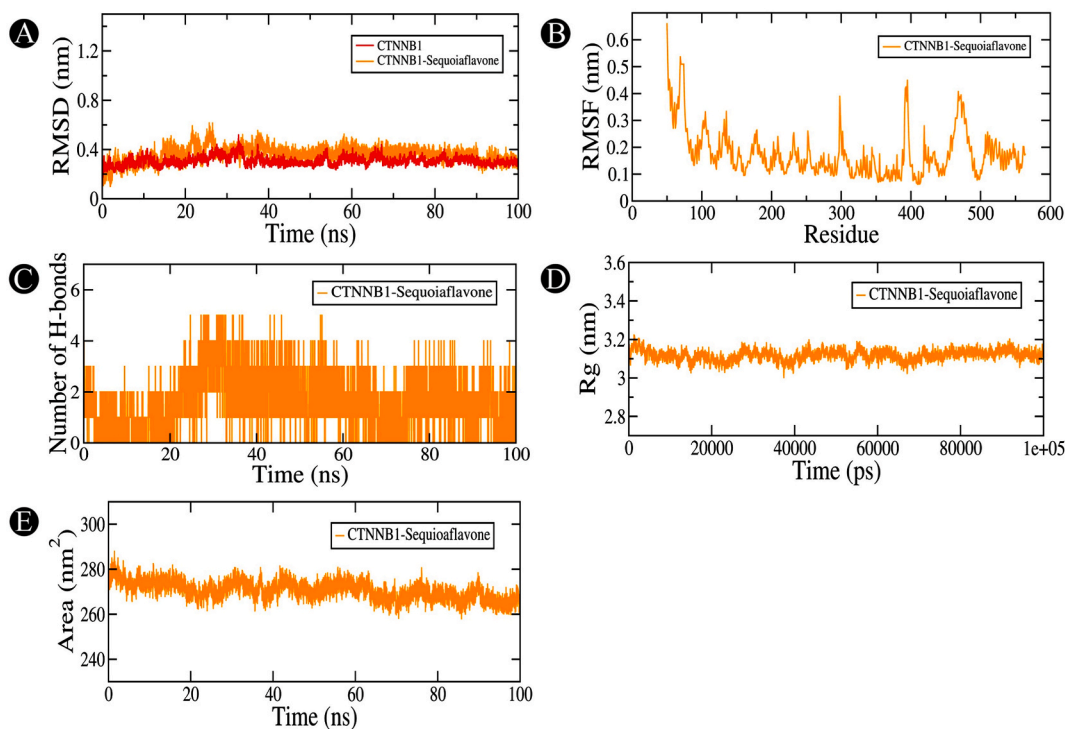


Fig. 14. The molecular dynamics simulation analysis of CTNNB1 protein and sequoiaflavone molecule over time. Molecular dynamics of CTNNB1 and its binding with sequoiaflavone. (A). RMSD analysis of CTNNB1 with and without sequoiaflavone binding, (B). RMSF analysis of CTNNB1-sequoiaflavone complex, (C). CTNNB1-sequoiaflavone complex intermolecular H-bond time evolution within 0.35 nm, (D). The Rg distribution of CTNNB1-sequoiaflavone complex, (E). SASA plot analysis of CTNNB1-sequoiaflavone complex.

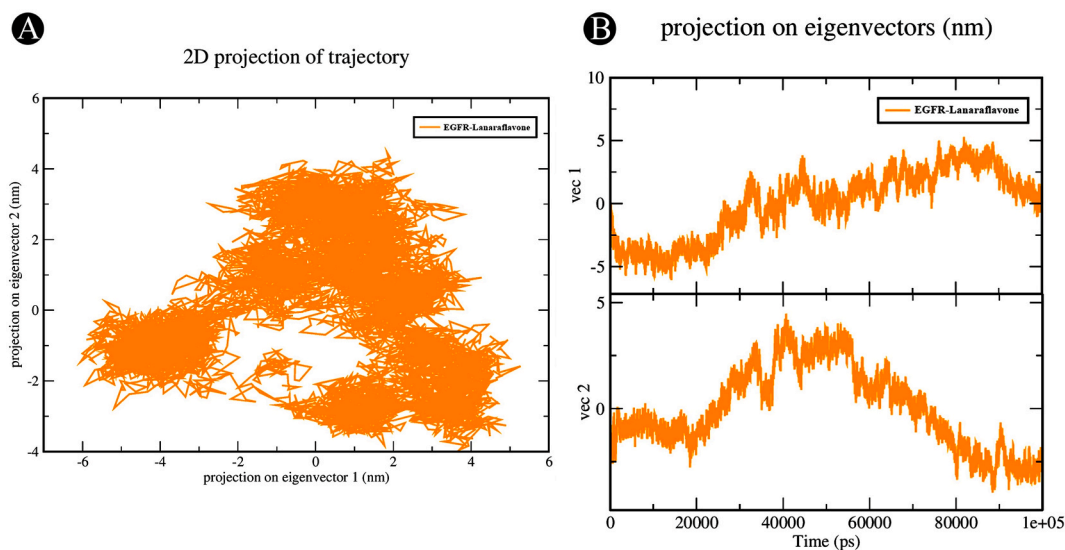


Fig. 15. Conformational projections of EGFR in PCA. (A). 2D projections of conformational sampling of EGFR-lanaroflavone. (B). The time evolution of projections of trajectories on both EVs.

target proteins [95]. The ADMET and toxicity analyses provided valuable insight into the pharmacokinetics and safety profile of the lead compounds [96]. A significant step towards selecting potential therapeutic candidates involves the identification of ligands with favourable ADMET properties [97]. In addition, molecular dynamics simulations can offer insight into the dynamic interactions between drugs and their target molecules, thus enabling a deeper understanding of their binding mechanisms, their stability and their interactions [98]. Therefore, the purpose of this study was to determine the efficacy of *S. bryopteris* phytochemical constituents by

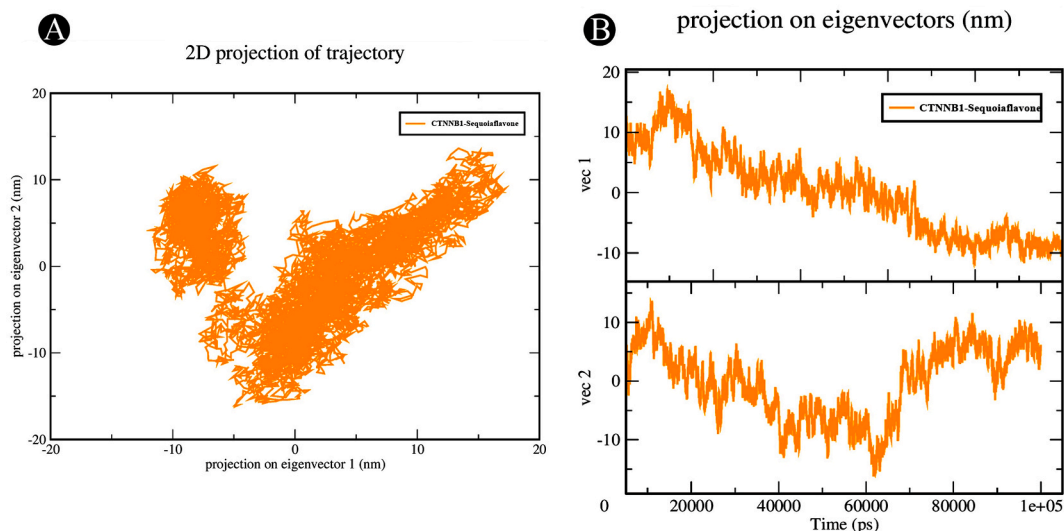


Fig. 16. Conformational projections of CTNNB1 in PCA. (A). 2D projections of conformational sampling of CTNNB1-sequoiaflavone. (B). The time evolution of projections of trajectories on both EVs.

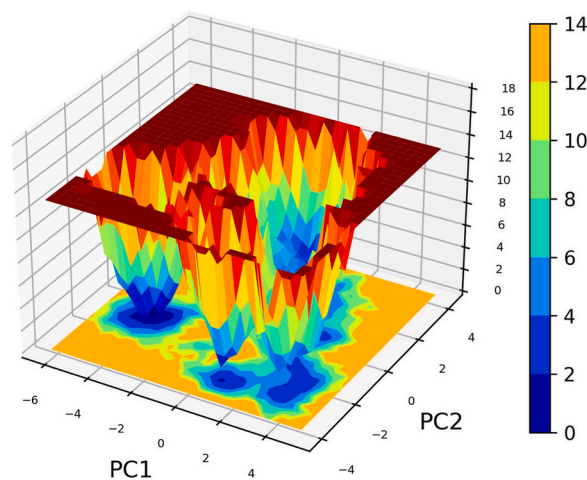


Fig. 17. The FEL plots for EGFR-lanaroflavone complex.

screening them and determining the binding stability between them and the central targets. In a molecular dynamics analysis, with a temperature of 300 K and a pressure of 1 atm, lanaroflavone-EGFR and sequoiaflavone-CTNNB1 showed stable conformations in solvation in water. The results of the docking analysis are consistent with what has been shown in the molecular dynamics analysis. The RMSD analysis confirmed the stability of both complexes over time, showing minimal structural fluctuations. RMSF analysis further revealed that key binding residues exhibited limited flexibility, indicating stable interactions. Hydrogen bond analysis demonstrated consistent interactions between lanaroflavone-EGFR and sequoiaflavone-CTNNB1 and crucial residues of throughout the simulation, supporting the docking results. The Rg indicated that the complex maintained its compactness, while SASA analysis showed stable exposure to the solvent, suggesting a stable conformation of the complex in a biological environment. However, for further validation, future work could involve mutagenesis studies to target key residues of EGFR and CTNNB1 identified in the docking and MD simulations, allowing to assess how these alterations impact the binding of lanaroflavone and sequoiaflavone. Additionally, targeted inhibition assays such as biochemical or cell-based assays could be performed to experimentally verify the inhibitory effects of lanaroflavone and sequoiaflavone on EGFR and CTNNB1 activity, respectively. These experimental methods would provide direct evidence supporting the computational findings.

Moreover, in addition to the initial suggestion of EGFR as a potential therapeutic target, it is crucial to consider the broader context of EGFR function and its regulation. EGFR plays a central role in various signaling pathways that influence cell growth, survival and proliferation. Therefore, targeting EGFR requires a comprehensive understanding of the other critical pathways that interact with or regulate EGFR activity [99,100]. Several key signaling pathways can modulate EGFR function. Notably, the PI3K/AKT pathway is

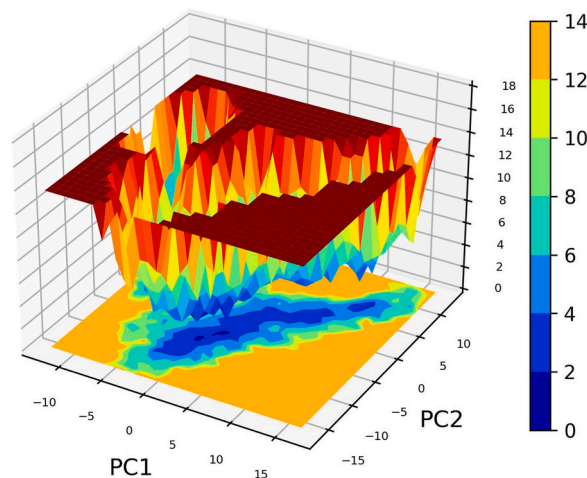


Fig. 18. The FEL plots for CTNNB1-sequoiaflavone complex.

frequently activated in conjunction with EGFR signaling. The PI3K/AKT pathway contributes to cell survival and proliferation and its activation can enhance EGFR signaling or even compensate for its inhibition. Thus, the efficacy of targeting EGFR might be influenced by the concurrent activation of this pathway [101]. Similarly, the MAPK pathway is another critical signaling cascade often associated with EGFR. This pathway is involved in transmitting signals from the cell surface to the nucleus, affecting gene expression related to cell growth and differentiation. Alterations in MAPK signaling can impact EGFR function and may influence the outcome of EGFR-targeted therapies. The therapeutic potential of targeting EGFR is also impacted by the presence of competitive inhibitors [102]. Tyrosine kinase inhibitors (TKIs), such as gefitinib and erlotinib are designed to specifically inhibit EGFR activity. However, the presence of other TKIs or small molecules that target different kinases can affect the effectiveness of EGFR inhibitors [103]. Additionally, the development of resistance to these inhibitors can diminish their therapeutic efficacy. Considering these factors, the therapeutic potential of *S. bryopteris* in targeting EGFR should be evaluated in the context of its interactions with these pathways and competitive inhibitors. An effective EGFR-targeting strategy might require a combination approach, addressing not only EGFR but also modulating the associated signaling pathways and overcoming resistance mechanisms.

An analysis of the anticancer and antimetastatic effects of *S. bryopteris* crude extract on breast cancer cells was conducted to confirm the anticancer activity. Antioxidant, anti-inflammation, chemopreventive and anticancer properties of *S. bryopteris* crude extract are reported [98,104]. There has been report that flavonoid-rich fraction of *S. bryopteris* showed anticarcinogenic and chemopreventive potential *in-vitro* and *in-vivo*. Mishra et al., reported the antioxidant, anti-inflammatory, anti-apoptotic and genoprotective effects of flavonoids of *S. bryopteris* [105]. MTT assays is a common method to determine the cytotoxic potential of any compound [106]. The obtained results of MTT assay revealed that *S. bryopteris* crude extract had cytotoxic effects after 24 h of treatment against human breast cancer cells. Moreover, one of the most challenging aspects of cancer treatment is metastasis, which occurs when cancer cells spread from the primary tumor to distant sites. It is the leading cause of cancer-related death worldwide [107]. Metastasis mechanisms need to be understood and targeted in order to develop effective anti-metastatic therapies [108]. Therefore, the aim of this study is to further explore the anti-metastatic potential of crude extract of *S. bryopteris* and discuss its implications for the treatment of cancer. In breast cancer cells, *S. bryopteris* crude extract showed a promising anti-metastatic effect. The treatment of breast cancer cells with *S. bryopteris* significantly reduced the migration and invasion of cancer cells in both wound healing and invasion assays.

Overall, integrated approach utilized in the present study shed light on the promising potential of *S. bryopteris* in combating breast cancer. The present study synergizes the strengths of both computational and experimental techniques, leading to more reliable and comprehensive findings. The network pharmacology component provides a systems-level view of potential molecular targets and interactions. By analyzing networks of protein-protein interactions, pathways and bioactive compounds identification of key targets and mechanisms that might be involved in the therapeutic effects of *S. bryopteris*. This theoretical framework is crucial for predicting which targets are most likely to be affected by the compound. *In vitro* assays complement these predictions by providing empirical evidence of the *S. bryopteris* effects on specific biological systems. These assays test the actual biological activity in a controlled environment, validating the theoretical predictions made by network pharmacology. This cross-validation between computational predictions and experimental results enhances the overall reliability of our findings. To illustrate the effectiveness of this integrated approach, we refer to several successful studies in the literature. For instance, a study by Wu et al. (2024) [109] combined network pharmacology with *in vitro* assays to identify and validate novel targets for colorectal cancer treatment from Qi-Qin-Hu—Chang formula demonstrating how such an approach can lead to significant discoveries in drug development. Similarly, Zhou et al. (2024) [110] used a combined methodology to explore the therapeutic potential of naringenin against cervical treatment, showcasing the benefits of integrating computational predictions with experimental validation. These examples highlight how the integration of network pharmacology with experimental assays can enhance the accuracy and reliability of therapeutic evaluations, supporting the effectiveness of our approach in the study of *S. bryopteris*. However, the comprehensive analysis presented in the present study

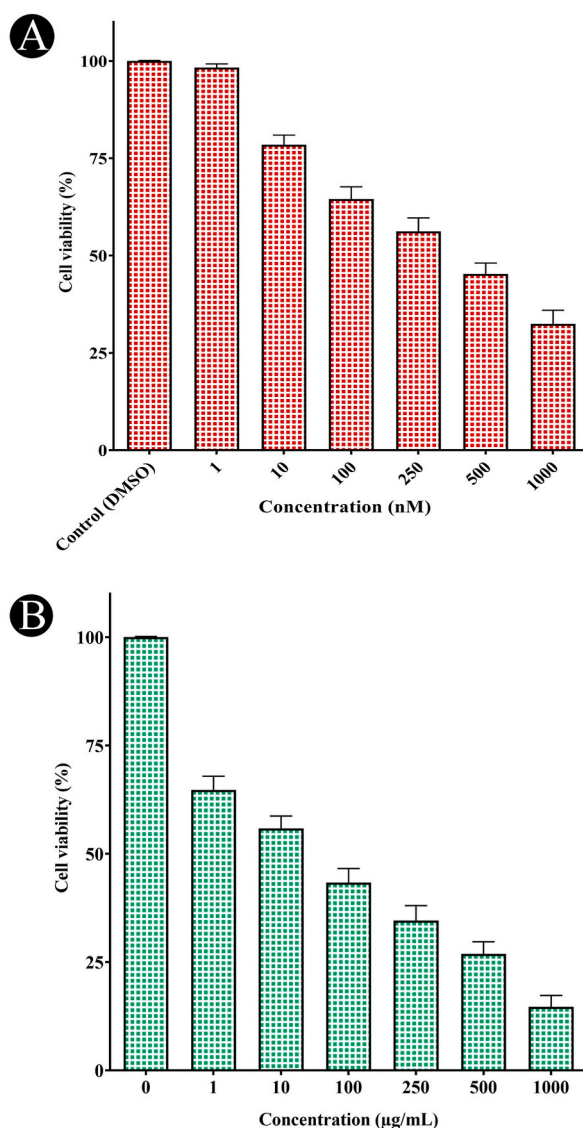


Fig. 19. Effect of Paclitaxel (standard drug) and *S. bryopteris* crude extract on cell viability (%) of MCF-7 cells determined via MTT assay. (A). Cell viability (%) of MCF-7 cells in presence of DMSO (negative control) and different concentration of Paclitaxel (standard drug) after 24 h, (B). Cell viability (%) of MCF-7 cells in presence of different concentration of *S. bryopteris* crude extract after 24 h. Each value represents the mean of three independent experiments conducted in triplicate.

highlights the need for further research and clinical investigations to harness the therapeutic benefits of this natural compounds. With its multifaceted mechanisms of action, *S. bryopteris* may hold the key to developing innovative and effective treatments for breast cancer, offering hope for improved patient outcomes and a brighter future in the fight against this devastating disease.

5. Conclusion

A multidisciplinary approach combining network pharmacology, molecular docking, molecular dynamics simulations and *in-vitro* validation utilized in the present study has provided compelling evidence of the potential therapeutic utility of *S. bryopteris* in breast cancer management. Through a systematic exploration of its molecular interactions and biological activity, present study uncovered key mechanisms by which *S. bryopteris* components may exert anticancer effects. Results of the present study suggest that *S. bryopteris* has the potential to target multiple signaling pathways implicated in breast cancer progression, including cell proliferation, metastasis and angiogenesis. The results of molecular docking and dynamics simulations identified specific compounds within *S. bryopteris* may interact with critical oncogenic targets, presenting an avenue for further drug development. The *in-vitro* experiments have verified our computational predictions, demonstrating the ability of *S. bryopteris* crude extract to inhibit breast cancer cell growth and metastasis. Hence, the present study shows the possibility of *S. bryopteris* and its compounds as a useful source of new therapeutic agents or as an

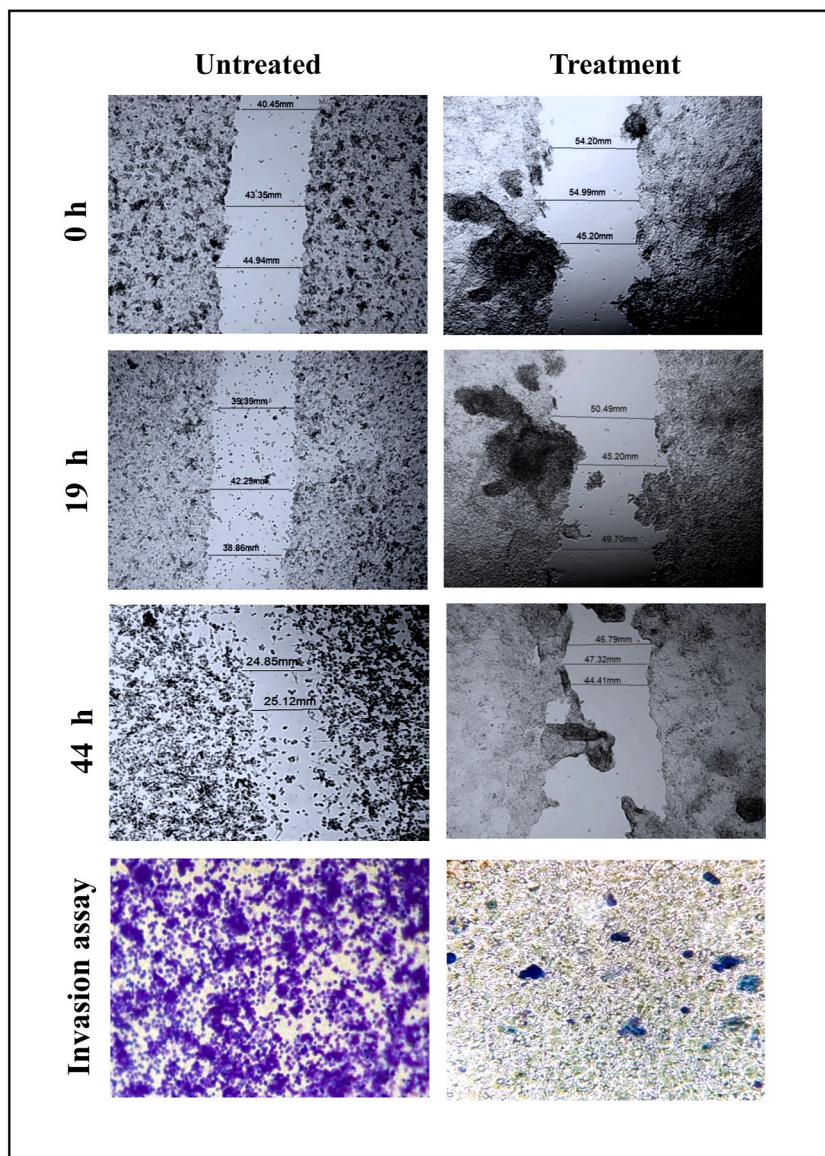


Fig. 20. The effect of *S. bryopteris* crude extract on the migration of MCF-7 cells at 0 h, 19 h and 44 h as well as invasion of cells after treatment with IC_{50} concentration.

adjunctive treatment option in breast cancer therapy. The crude extract or compounds of *S. bryopteris* show significant efficacy against cancer targets while potentially offering lower toxicity compared to existing therapies. This suggests that they could lead to novel, safer and more effective anticancer drugs. However, further investigations including preclinical and clinical trials, are necessary to fully elucidate the safety, efficacy and dosage requirements of *S. bryopteris* based interventions. Additionally, exploring the synergy of *S. bryopteris* with existing treatments and its potential in other cancer types could expand its therapeutic scope.

Funding

This research has been funded by Deputy for Research & Innovation, Ministry of Education through Initiative of Institutional Funding at University of Ha'il-Saudi Arabia through project number IFP-22113.

Ethical approval

The taxonomic identification of the plant material was carried out by a Pteridologist and Botanist Dr. Mitesh Patel. Further, no other ethical approval was sought for the present study and is Not Applicable, because this article does not contain any studies with

human or animal subjects.

Data availability statement

The information supporting this study is available in this article.

CRediT authorship contribution statement

Amir Mahgoub Awadelkareem: Writing – original draft, Validation, Funding acquisition, Formal analysis, Data curation, Conceptualization. **Mitesh Patel:** Writing – review & editing, Validation, Software, Methodology, Formal analysis, Data curation. **Humera Banu:** Writing – review & editing, Validation, Methodology, Investigation, Formal analysis, Data curation. **Mohd Adnan:** Writing – review & editing, Writing – original draft, Supervision, Project administration, Formal analysis, Conceptualization.

Declaration of competing interest

The authors declare the following financial interests/personal relationships which may be considered as potential competing interests: Mohd Adnan is currently serving as an AE in this journal. If there are other authors, they declare that they have no known competing financial interests or personal relationships that could have appeared to influence the work reported in this paper.

Acknowledgements

This research has been funded by Deputy for Research & Innovation, Ministry of Education through Initiative of Institutional Funding at University of Ha'il-Saudi Arabia through project number IFP-22113.

References

- [1] S.C. Houghton, S.E. Hankinson, Cancer progress and priorities: breast cancer, *Cancer Epidemiol. Biomarkers Prev.* 30 (5) (2021) 822–844.
- [2] Y. Liu, R.M. Tamimi, L.C. Collins, et al., The association between vascular endothelial growth factor expression in invasive breast cancer and survival varies with intrinsic subtypes and use of adjuvant systemic therapy: results from the Nurses' Health Study, *Breast Cancer Res. Treat.* 129 (2011) 175–184.
- [3] M. Arnold, E. Morgan, H. Rungay, et al., Current and future burden of breast cancer: global statistics for 2020 and 2040, *Breast* 66 (2022) 15–23.
- [4] S. Łukasiewicz, M. Czezelewski, A. Forma, J. Baj, R. Sitarz, A. Stanisławek, Breast cancer—epidemiology, risk factors, classification, prognostic markers, and current treatment strategies—an updated review, *Cancers* 13 (17) (2021) 4287.
- [5] F.K. Al-Thoubaity, Molecular classification of breast cancer: a retrospective cohort study, *Annals of medicine and surgery* 49 (2020) 44–48.
- [6] S. Lopez-Tarruella, I. Echavarría, Y. Jerez, B. Herrero, S. Gamez, M. Martin, How we treat HR-positive, HER2-negative early breast cancer, *Future Oncol.* 18 (8) (2022) 1003–1022.
- [7] S.S. Bashraheel, A. Domling, S.K. Goda, Update on targeted cancer therapies, single or in combination, and their fine tuning for precision medicine, *Biomed. Pharmacother.* 125 (2020) 110009.
- [8] E.-Y. Ko, A. Moon, Natural products for chemoprevention of breast cancer, *Journal of cancer prevention* 20 (4) (2015) 223.
- [9] Y. Li, S. Li, X. Meng, R.-Y. Gan, J.-J. Zhang, H.-B. Li, Dietary natural products for prevention and treatment of breast cancer, *Nutrients* 9 (7) (2017) 728.
- [10] S. Mitra, R. Dash, Natural products for the management and prevention of breast cancer, *Evid. base Compl. Alternative Med.* 2018 (2018).
- [11] U. Anand, N. Jacobo-Herrera, A. Altemimi, N. Lakhssassi, A comprehensive review on medicinal plants as antimicrobial therapeutics: potential avenues of biocompatible drug discovery, *Metabolites* 9 (11) (2019) 258.
- [12] S.A. Rizvi, G.P. Einstein, O.L. Tulp, F. Sainvil, R. Branly, Introduction to traditional medicine and their role in prevention and treatment of emerging and re-emerging diseases, *Biomolecules* 12 (10) (2022) 1442.
- [13] A.G. Atanasov, S.B. Zotchev, V.M. Dirsch, C.T. Supuran, Natural products in drug discovery: advances and opportunities, *Nat. Rev. Drug Discov.* 20 (3) (2021) 200–216.
- [14] J. Hong, Role of natural product diversity in chemical biology, *Curr. Opin. Chem. Biol.* 15 (3) (2011) 350–354.
- [15] S. Hashem, T.A. Ali, S. Akhtar, et al., Targeting cancer signaling pathways by natural products: exploring promising anti-cancer agents, *Biomed. Pharmacother.* 150 (2022) 113054.
- [16] M. Riaz, R. Khalid, M. Afzal, et al., Phytobioactive compounds as therapeutic agents for human diseases: a review, *Food Sci. Nutr.* 11 (6) (2023) 2500–2529.
- [17] A. Roy, A. Khan, I. Ahmad, et al., Flavonoids a bioactive compound from medicinal plants and its therapeutic applications, *BioMed Res. Int.* 2022 (2022).
- [18] A.M. Seca, D.C. Pinto, Plant secondary metabolites as anticancer agents: successes in clinical trials and therapeutic application, *Int. J. Mol. Sci.* 19 (1) (2018) 263.
- [19] S. Shweta, R. Singh, T. Sahu, *Floral Diversity and Their Conservation*, Publisher Biotech Book., 2013, pp. 267–290.
- [20] S. Singh, R. Singh, Ethnomedicinal use of Pteridophytes in reproductive health of tribal women of Pachmarhi Biosphere Reserve, Madhya Pradesh, India, *Int. J. Pharmaceut. Sci. Res.* 3 (12) (2012) 4780.
- [21] S.K. Paswan, A. Gautam, P. Verma, et al., The Indian magical herb 'Sanjeevani' (Selaginella bryopteris L.)—A promising anti-inflammatory phytomedicine for the treatment of patients with inflammatory skin diseases, *J. Pharmacopuncture* 20 (2) (2017) 93.
- [22] S. Agarwal, V. Singh, Immunomodulators: a review of studies on Indian medicinal plants and synthetic peptides. Part-I: medicinal plants, *Proceedings of the Indian National Science Academy-Part B: Biological Sciences* 65 (3–4) (1999) 179–204.
- [23] J. Chandrakant, P. Mathad, S. Mety, M. Ahmed, M. Sanaullah, Phytochemical and Antidepressant Activities of Selaginella Bryopteris (L.) Baker on Albino Mice, 2015.
- [24] R. Kumari, J. Singh, P. Kumari, A. Jha, Impact of Selaginella bryopteris on biochemical analysis of diabetic swiss albino mice caused induced by alloxan, *Int J Basic Appl Sci Res.* 1 (2) (2014) 95–99.
- [25] K. Miki, T. Nagai, T. Nakamura, et al., Synthesis and evaluation of influenza virus sialidase inhibitory activity of hinokiflavone-sialic acid conjugates, *Heterocycles* 75 (4) (2008) 879–886.
- [26] P. Rupa, N.L. Bhavani, Preliminary phytochemical screening of desiccated Fronds of Selaginellabryopteris (L.) baker (pittakalu), *World J Pharm Sci* 3 (9) (2014) 1370–1378.
- [27] P. Sah, Does the magical himalayan herb "Sanjeevani Booti" really exist in nature, *The Journal of American Science* 4 (3) (2008), 1545–1003.
- [28] A.M. Elsbali, W.A. Al-Soud, A.E. Mousa Elayyan, et al., Integrating network pharmacology approaches for the investigation of multi-target pharmacological mechanism of 6-shogaol against cervical cancer, *J. Biomol. Struct. Dyn.* 41 (23) (2023) 14135–14151.

- [29] M. Adnan, A.J. Siddiqui, E. Noumi, et al., Integrating network pharmacology approaches to decipher the multi-target pharmacological mechanism of microbial biosurfactants as novel green antimicrobials against listeriosis, *Antibiotics* 12 (1) (2022) 5.
- [30] P. Poornima, J.D. Kumar, Q. Zhao, M. Blunder, T. Efferth, Network pharmacology of cancer: from understanding of complex interactomes to the design of multi-target specific therapeutics from nature, *Pharmacol. Res.* 111 (2016) 290–302.
- [31] D. Gfeller, O. Michielin, V. Zoete, Shaping the interaction landscape of bioactive molecules, *Bioinformatics* 29 (23) (2013) 3073–3079.
- [32] G. Xiong, Z. Wu, J. Yi, et al., ADMETlab 2.0: an integrated online platform for accurate and comprehensive predictions of ADMET properties, *Nucleic Acids Res.* 49 (W1) (2021) W5–W14.
- [33] E.M. Gad, M.S. Nafee, E.H. Eltamany, M.S. Hammad, A. Barakat, A.T. Boraie, Discovery of new apoptosis-inducing agents for breast cancer based on ethyl 2-amino-4, 5, 6, 7-tetra hydrobenzo [b] thiophene-3-carboxylate: synthesis, in vitro, and in vivo activity evaluation, *Molecules* 25 (11) (2020) 2523.
- [34] M. Pathan, S. Keerthikumar, C.S. Ang, et al., FunRich: an open access standalone functional enrichment and interaction network analysis tool, *Proteomics* 15 (15) (2015) 2597–2601.
- [35] J. Piñero, J.M. Ramírez-Angueta, J. Saüch-Pitarch, et al., The DisGeNET knowledge platform for disease genomics: 2019 update, *Nucleic Acids Res.* 48 (D1) (2020) D845–D855.
- [36] D. Szklarczyk, A.L. Gable, K.C. Nastou, et al., The STRING database in 2021: customizable protein–protein networks, and functional characterization of user-uploaded gene/measurement sets, *Nucleic Acids Res.* 49 (D1) (2021) D605–D612.
- [37] P. Shannon, A. Markiel, O. Ozier, et al., Cytoscape: a software environment for integrated models of biomolecular interaction networks, *Genome Res.* 13 (11) (2003) 2498–2504.
- [38] B.T. Sherman, D.W. Huang, Q. Tan, et al., DAVID Knowledgebase: a gene-centered database integrating heterogeneous gene annotation resources to facilitate high-throughput gene functional analysis, *BMC Bioinf.* 8 (2007) 1–11.
- [39] G.M. Morris, R. Huey, A.J. Olson, Using autodock for ligand-receptor docking, *Current protocols in bioinformatics* 24 (1) (2008), 8.14. 1–8.14. 40.
- [40] N.M. O’Boyle, M. Banck, C.A. James, C. Morley, T. Vandermeersch, G.R. Hutchison, Open Babel: an open chemical toolbox, *J. Cheminf.* 3 (2011) 1–14.
- [41] D. Studio, *Discovery Studio*, 2008, p. 420. *Accelrys [21]*.
- [42] M. Adnan, A. Shamsi, A.M. Elsbali, et al., Structure-guided approach to discover tuberosin as a potent activator of pyruvate kinase M2, targeting cancer therapy, *Int. J. Mol. Sci.* 23 (21) (2022) 13172.
- [43] A.H. Bahaman, R.A. Wahab, A.A. Abdul Hamid, K.B. Abd Halim, Y. Kaya, Molecular docking and molecular dynamics simulations studies on β -glucosidase and xylanase *Trichoderma asperellum* to predict degradation order of cellulosic components in oil palm leaves for nanocellulose preparation, *J. Biomol. Struct. Dyn.* 39 (7) (2021) 2628–2641.
- [44] N. Bouali, I. Ahmad, H. Patel, et al., GC–MS screening of the phytochemical composition of Ziziphus honey: ADME properties and in vitro/in silico study of its antimicrobial activity, *J. Biomol. Struct. Dyn.* (2023) 1–13.
- [45] S. Páll, M.J. Abraham, C. Kutzner, B. Hess, E. Lindahl, Tackling Exascale Software Challenges in Molecular Dynamics Simulations with GROMACS, Springer, 2015, pp. 3–27.
- [46] M.J. Abraham, T. Murtola, R. Schulz, et al., GROMACS: high performance molecular simulations through multi-level parallelism from laptops to supercomputers, *SoftwareX* 1 (2015) 19–25.
- [47] M. Adnan, A.J. Siddiqui, S.A. Ashraf, et al., Network pharmacology, molecular docking, and molecular dynamics simulation to elucidate the molecular targets and potential mechanism of *Phoenix dactylifera* (ajwa dates) against candidiasis, *Pathogens* 12 (11) (2023) 1369.
- [48] N.M. Alotaibi, M.O. Alotaibi, N. Alshammari, M. Adnan, M. Patel, Network pharmacology combined with molecular docking, molecular dynamics, and in vitro experimental validation reveals the therapeutic potential of thymus vulgaris L. Essential oil (thyme oil) against human breast cancer, *ACS Omega* 8 (50) (2023) 48344–48359.
- [49] T. Mohammad, S. Siddiqui, A. Shamsi, et al., Virtual screening approach to identify high-affinity inhibitors of serum and glucocorticoid-regulated kinase 1 among bioactive natural products: combined molecular docking and simulation studies, *Molecules* 25 (4) (2020) 823.
- [50] A. Altis, M. Otten, P.H. Nguyen, R. Hegger, G. Stock, Construction of the free energy landscape of biomolecules via dihedral angle principal component analysis, *J. Chem. Phys.* 128 (24) (2008).
- [51] S. Genheden, U. Ryde, The MM/PBSA and MM/GBSA methods to estimate ligand-binding affinities, *Expert Opin. Drug Discov.* 10 (5) (2015) 449–461.
- [52] R. Kumari, R. Kumar, O.S.D.D. Consortium, A. Lynn, g_mmpbsa A GROMACS tool for high-throughput MM-PBSA calculations, *J. Chem. Inf. Model.* 54 (7) (2014) 1951–1962.
- [53] M. Richter, O. Piwocka, M. Musielak, I. Piotrowski, W.M. Suchorska, T. Trzeciak, From donor to the lab: a fascinating journey of primary cell lines, *Front. Cell Dev. Biol.* 9 (2021) 711381.
- [54] F.M. Freimoser, C.A. Jakob, M. Aebi, U. Tuor, The MTT [3-(4, 5-dimethylthiazol-2-yl)-2, 5-diphenyltetrazolium bromide] assay is a fast and reliable method for colorimetric determination of fungal cell densities, *Appl. Environ. Microbiol.* 65 (8) (1999) 3727–3729.
- [55] J.A. Plumb, Cell sensitivity assays: the MTT assay, *Cancer cell culture: methods and protocols* (2004) 165–169.
- [56] J.E. Jonkman, J.A. Cathcart, F. Xu, et al., An introduction to the wound healing assay using live-cell microscopy, *Cell Adhes. Migrat.* 8 (5) (2014) 440–451.
- [57] C.R. Justus, M.A. Marie, E.J. Sanderlin, L.V. Yang, Transwell in vitro cell migration and invasion assays. *Cell Viability Assays: Methods and Protocols*, Springer, 2023, pp. 349–359.
- [58] G.B. Maru, R.R. Hudlikar, G. Kumar, K. Gandhi, M.B. Mahimkar, Understanding the molecular mechanisms of cancer prevention by dietary phytochemicals: from experimental models to clinical trials, *World J. Biol. Chem.* 7 (1) (2016) 88.
- [59] D.J. Huggins, P.C. Biggin, M.A. Dämgén, et al., Biomolecular simulations: from dynamics and mechanisms to computational assays of biological activity, *Wiley Interdiscip. Rev. Comput. Mol. Sci.* 9 (3) (2019) e1393.
- [60] T. Schlick, R. Collepardo-Guevara, L.A. Halvorsen, S. Jung, X. Xiao, Biomolecular modeling and simulation: a field coming of age, *Q. Rev. Biophys.* 44 (2) (2011) 191–228.
- [61] T. Schlick, S. Portillo-Ledesma, C.G. Myers, et al., Biomolecular modeling and simulation: a prospering multidisciplinary field, *Annu. Rev. Biophys.* 50 (2021) 267–301.
- [62] S. Mondal, B. Bagchi, From structure and dynamics to biomolecular functions: the ubiquitous role of solvent in biology, *Curr. Opin. Struct. Biol.* 77 (2022) 102462.
- [63] T. Schlick, T. Schlick, Biomolecular structure and modeling: historical perspective, *Molecular Modeling and Simulation: An Interdisciplinary Guide: An Interdisciplinary Guide* (2010) 1–40.
- [64] X. Xu, A. Liu, S. Liu, et al., Application of molecular dynamics simulation in self-assembled cancer nanomedicine, *Biomater. Res.* 27 (1) (2023) 39.
- [65] A. Bojja, I.A. Klein, R.A. Young, Biomolecular condensates and cancer, *Cancer Cell* 39 (2) (2021) 174–192.
- [66] B. Dale, M. Cheng, K.-S. Park, H.Ü. Kaniskan, Y. Xiong, J. Jin, Advancing targeted protein degradation for cancer therapy, *Nat. Rev. Cancer* 21 (10) (2021) 638–654.
- [67] A.A. Ivanov, F.R. Khuri, H. Fu, Targeting protein–protein interactions as an anticancer strategy, *Trends Pharmacol. Sci.* 34 (7) (2013) 393–400.
- [68] A. Wolska-Washer, P. Smolewski, Targeting protein degradation pathways in tumors: focusing on their role in hematological malignancies, *Cancers* 14 (15) (2022) 3778.
- [69] M. Adnan, M. Patel, M. Snoussi, *Ethnobotany and Ethnopharmacology of Medicinal and Aromatic Plants: Steps towards Drug Discovery*, CRC Press, 2023.
- [70] J.-Y. Ortholand, A. Ganesan, Natural products and combinatorial chemistry: back to the future, *Curr. Opin. Chem. Biol.* 8 (3) (2004) 271–280.
- [71] M. Dickson, J.P. Gagnon, Key factors in the rising cost of new drug discovery and development, *Nat. Rev. Drug Discov.* 3 (5) (2004) 417–429.
- [72] S. Lu, Y. Qiu, D. Ni, X. He, J. Pu, J. Zhang, Emergence of allosteric drug-resistance mutations: new challenges for allosteric drug discovery, *Drug Discov. Today* 25 (1) (2020) 177–184.
- [73] A. Ribas, P. Hersey, M.R. Middleton, et al., New challenges in endpoints for drug development in advanced melanoma, *Clin. Cancer Res.* 18 (2) (2012) 336–341.

- [74] T. Utsugi, New challenges and inspired answers for anticancer drug discovery and development, *Jpn. J. Clin. Oncol.* 43 (10) (2013) 945–953.
- [75] A.L. Hopkins, Network pharmacology: the next paradigm in drug discovery, *Nat. Chem. Biol.* 4 (11) (2008) 682–690.
- [76] L.C. Pal, A. Gautam, V. Pande, C.V. Rao, Anticancer property of *Selaginella bryopteris* (L.) Bak. against hepatocellular carcinoma in vitro and in vivo, *Phytomedicine* 2 (1) (2022) 100201.
- [77] H. Masuda, D. Zhang, C. Bartholomeusz, H. Doihara, G.N. Hortobagyi, N.T. Ueno, Role of epidermal growth factor receptor in breast cancer, *Breast Cancer Res. Treat.* 136 (2012) 331–345.
- [78] C. Magkou, L. Nakopoulou, C. Zoubouli, et al., Expression of the epidermal growth factor receptor (EGFR) and the phosphorylated EGFR in invasive breast carcinomas, *Breast Cancer Res.* 10 (2008) 1–8.
- [79] X. Song, Z. Liu, Z. Yu, EGFR promotes the development of triple negative breast cancer through JAK/STAT3 signaling, *Cancer Manag. Res.* (2020) 703–717.
- [80] M. Gasco, S. Shami, T. Crook, The p53 pathway in breast cancer, *Breast Cancer Res.* 4 (2002) 1–7.
- [81] Y. Du, J. Zhang, Y. Meng, M. Huang, W. Yan, Z. Wu, MicroRNA-143 targets MAPK3 to regulate the proliferation and bone metastasis of human breast cancer cells, *Amb. Express* 10 (2020) 1–8.
- [82] A. Livshits, A. Git, G. Fuks, C. Caldas, E. Domany, Pathway-based personalized analysis of breast cancer expression data, *Mol. Oncol.* 9 (7) (2015) 1471–1483.
- [83] J-h Ma, L. Qin, X. Li, Role of STAT3 signaling pathway in breast cancer, *Cell Commun. Signal.* 18 (2020) 1–13.
- [84] S.G. Manore, D.L. Doheny, G.L. Wong, H.-W. Lo, IL-6/JAK/STAT3 signaling in breast cancer metastasis: biology and treatment, *Front. Oncol.* 12 (2022) 866014.
- [85] S.Q. To, R.S. Dmello, A.K. Richards, M. Ernst, A.L. Chand, STAT3 signaling in breast cancer: multicellular actions and therapeutic potential, *Cancers* 14 (2) (2022) 429.
- [86] H. Al Kawas, I. Saaid, P. Jank, et al., How VEGF-A and its splice variants affect breast cancer development—clinical implications, *Cell. Oncol.* 45 (2) (2022) 227–239.
- [87] D. Cruceriu, O. Baldasici, O. Balacescu, I. Berindan-Neagoe, The dual role of tumor necrosis factor-alpha (TNF- α) in breast cancer: molecular insights and therapeutic approaches, *Cell. Oncol.* 43 (2020) 1–18.
- [88] J.O. Brett, L.M. Spring, A. Bardia, S.A. Wander, ESRI mutation as an emerging clinical biomarker in metastatic hormone receptor-positive breast cancer, *Breast Cancer Res.* 23 (2021) 1–15.
- [89] X. Xu, M. Zhang, F. Xu, S. Jiang, Wnt signaling in breast cancer: biological mechanisms, challenges and opportunities, *Mol. Cancer* 19 (1) (2020) 165.
- [90] B. George, B. Gui, R. Raguraman, et al., AKT1 transcriptomic landscape in breast cancer cells, *Cells* 11 (15) (2022) 2290.
- [91] F. Martorana, G. Motta, G. Pavone, et al., AKT inhibitors: new weapons in the fight against breast cancer? *Front. Pharmacol.* 12 (2021) 662232.
- [92] J. Luo, H. Zou, Y. Guo, et al., SRC kinase-mediated signaling pathways and targeted therapies in breast cancer, *Breast Cancer Res.* 24 (1) (2022) 99.
- [93] L. Chen, B. Fang, L. Qiao, Y. Zheng, Discovery of anticancer activity of amentoflavone on esophageal squamous cell carcinoma: bioinformatics, structure-based virtual screening, and biological evaluation, *J. Microbiol. Biotechnol.* 32 (6) (2022) 718.
- [94] J.-F. Goossens, L. Goossens, C. Bailly, Hinokiflavone and related C–O–C-type biflavonoids as anti-cancer compounds: properties and mechanism of action, *Natural Products and Bioprospecting* 11 (2021) 365–377.
- [95] R. Acharya, S. Chacko, P. Bose, A. Lapenna, S.P. Pattanayak, Structure based multitargeted molecular docking analysis of selected furanocoumarins against breast cancer, *Sci. Rep.* 9 (1) (2019) 15743.
- [96] M.M. Hasan, Z. Khan, M.S. Chowdhury, M.A. Khan, M.A. Moni, M.H. Rahman, In silico molecular docking and ADME/T analysis of Quercetin compound with its evaluation of broad-spectrum therapeutic potential against particular diseases, *Inform. Med. Unlocked* 29 (2022) 100894.
- [97] L. Guan, H. Yang, Y. Cai, et al., ADMET-score—a comprehensive scoring function for evaluation of chemical drug-likeness, *Medchemcomm* 10 (1) (2019) 148–157.
- [98] M. De Vivo, M. Masetti, G. Bottegoni, A. Cavalli, Role of molecular dynamics and related methods in drug discovery, *J. Med. Chem.* 59 (9) (2016) 4035–4061.
- [99] P. Seshacharyulu, M.P. Ponnusamy, D. Haridas, M. Jain, A.K. Ganti, S.K. Batra, Targeting the EGFR signaling pathway in cancer therapy, *Expert Opin. Ther. Targets* 16 (1) (2012) 15–31.
- [100] P. Wee, Z. Wang, Epidermal growth factor receptor cell proliferation signaling pathways, *Cancers* 9 (5) (2017) 52.
- [101] C. Freudspurger, J.R. Burnett, J.A. Friedman, V.R. Kannabiran, Z. Chen, C. Van Waes, EGFR–PI3K–AKT–mTOR signaling in head and neck squamous cell carcinomas: attractive targets for molecular-oriented therapy, *Expert Opin. Ther. Targets* 15 (1) (2011) 63–74.
- [102] W. Jiang, X. Wang, C. Zhang, L. Xue, L. Yang, Expression and clinical significance of MAPK and EGFR in triple-negative breast cancer, *Oncol. Lett.* 19 (3) (2020) 1842–1848.
- [103] R. Shah, J.F. Lester, Tyrosine kinase inhibitors for the treatment of EGFR mutation-positive non-small-cell lung cancer: a clash of the generations, *Clin. Lung Cancer* 21 (3) (2020) e216–e228.
- [104] M.H. Ansari, S.R. Walde, Phytochemical extraction and activity against *Salmonella typhi* of *Selaginella bryopteris*, *Int. J. Med. Pharmaceut. Sci.* 13 (2) (2023) 1.
- [105] P.K. Mishra, G.V. Raghuram, A. Bhargava, et al., In vitro and in vivo evaluation of the anticarcinogenic and cancer chemopreventive potential of a flavonoid-rich fraction from a traditional Indian herb *Selaginella bryopteris*, *Br. J. Nutr.* 106 (8) (2011) 1154–1168.
- [106] A. Bahuguna, I. Khan, V.K. Bajpai, S.C. Kang, MTT assay to evaluate the cytotoxic potential of a drug, *Bangladesh Journal of Pharmacology* 12 (2) (2017) 115–118.
- [107] S.D. Nathanson, M. Detmar, T.P. Padera, et al., Mechanisms of breast cancer metastasis, *Clin. Exp. Metastasis* 39 (1) (2022) 117–137.
- [108] M. Majumder, S. Debnath, R.L. Gajbhiye, et al., Ricinus communis L. fruit extract inhibits migration/invasion, induces apoptosis in breast cancer cells and arrests tumor progression in vivo, *Sci. Rep.* 9 (1) (2019) 14493.
- [109] Y. Wu, Y. Fang, Y. Li, et al., A network pharmacology approach and experimental validation to investigate the anticancer mechanism of Qi-Qin-Hu-Chang formula against colitis-associated colorectal cancer through induction of apoptosis via JNK/p38 MAPK signaling pathway, *J. Ethnopharmacol.* 319 (2024) 117323.
- [110] J. Zhou, H. Li, B. Wu, et al., Network pharmacology combined with experimental verification to explore the potential mechanism of naringenin in the treatment of cervical cancer, *Sci. Rep.* 14 (1) (2024) 1860.